https://doi.org/10.5194/egusphere-2026-2319
Preprint. Discussion started: 5 May 2026

Impact of Grid Resolution on the Abyssal Ocean Representation in Numerical Models: A Focus on Vema Channel

Daniel M. C. Santos[1], Mathias Van Caspel[2], Ralph Timmermann[2], and Olga T. Sato[1]

[1]Instituto Oceanográfico da Universidade de São Paulo, São Paulo, Brasil
[2]Alfred Wegener Institut, Helmholtz Zentrum für Polar und Meeresforschung, Bremerhaven, Germany.

Correspondence: Daniel M. C. Santos (daniel.melo.santos@alumni.usp.br)

Abstract.

Accurately representing abyssal water masses and their inter-basin pathways remains a challenge for global ocean models and reanalyses. In this study, we investigate how horizontal and vertical resolution influence the simulation of abyssal waters by first evaluating three ocean reanalyses and one forward ocean model, focusing on Antarctic Bottom Water pathways from the Weddell Sea to the Argentine and Brazil basins and through the Vema Channel. Model outputs are evaluated against WOA18 climatology and *in situ* observations from moorings and hydrographic sections. Based on these results, we conduct four targeted experiments with the Finite-Volume Sea Ice–Ocean Model (FESOM 2), modifying horizontal and vertical grid resolution while keeping all other model components unchanged. The experiments show that increasing vertical resolution substantially improves the representation of cold and dense abyssal waters and their inter-basin connectivity, whereas horizontal refinement alone does not systematically improve the representation of abyssal properties and can even degrade it when mixing parameterizations are not adequately tuned. Combining vertical and horizontal refinement improves specific local features, including the structure of the abyssal flow and the realistic eastward deflection of the Antarctic Bottom Water core within the Vema Channel, but does not outperform vertical refinement alone at the basin scale.

1 Introduction

The lower limb of the Atlantic Meridional Overturning Circulation (AMOC) is occupied by the Antarctic Bottom Water (AABW), a water mass which originates from dense waters formed on the Antarctic continental shelf, primarily within the Weddell Sea sector (Solodoch et al., 2022). There, Dense Shelf Water (DSW) descends the continental slope while entraining mid-depth modified Warm Deep Water (mWDW), forming two distinct water masses: The Weddell Sea Deep Water (WSDW) and the Weddell Sea Bottom Water (WSBW) (Orsi et al., 1999). WSBW is commonly limited, on its top, by the potential temperature (θ) isotherm of -0.7°C (Fahrbach et al., 1995). It remains largely confined to the Weddell Sea, without crossing the Scotia Ridge, although it can indirectly influence the properties of AABW exported to lower latitudes (Abrahamsen et al., 2019). The lighter WSDW overlies the WSBW within the Weddell Sea and is bounded by the $\theta = -0.7$°C (lower) and $\theta = 0.0$°C (upper) isotherms (Carmack, 1977). As WSDW overflows the South Scotia Ridge and enters the Scotia Sea, the ocean floor effectively becomes the lower boundary of WSDW outside the Weddell Sea (Fig. 1a)

https://doi.org/10.5194/egusphere-2026-2319
Preprint. Discussion started: 5 May 2026

The AABW variant which occupies the western South Atlantic is supplied precisely by the fraction of the WSDW that flows from the Scotia Sea into the southern Argentine Basin. Within the Argentine Basin, AABW is characterized by core properties of $\theta = -0.10$°C and salinity = 34.67 (Valla et al., 2018). Its upper limit is commonly identified by the potential density referenced to 4000 m depth (σ_4) isopycnal of 46.06 kg m^{-3} (Arhan et al., 1999), which corresponds to the $\theta = 0.0$°C isotherm. After entering the Argentine Basin, AABW spreads along the seafloor following several intricate and connected pathways and continues its northward propagation toward lower latitudes through the Vema Channel (Santos et al., 2025). This narrow passage acts as the principal conduit for AABW leaving the Argentine Basin and entering the Brazil Basin (Hogg et al., 1982; Morozov et al., 2018) before crossing the equator towards the North Atlantic Ocean. Due to the logistical complexity and high operational costs associated with sampling abyssal waters along deep boundary currents, basin interiors, and narrow passages such as the Vema Channel in a coordinated and simultaneous manner, sustained observations of this sector of the ocean are limited in both space and time.

Hence, despite substantial advances in the observational monitoring of the AMOC over the past decades, direct observations of its abyssal limb are sparse. The existing observational network relies on a combination of repeated full-depth conductivity–temperature–depth (CTD) sections and moored arrays. Ship-based hydrographic sections provide high-accuracy, full-depth snapshots of water mass properties, but they are intrinsically limited in time. In contrast, moored arrays offer continuous measurements, but their geographic coverage is limited, with most arrays concentrated near continental boundaries and restricted to a small number of latitudes.

In the Atlantic Ocean, sustained trans-basin moored arrays currently exist at only a few latitudes, including 11°S, 34.5°S, and 26.5°N, the TRopical Atlantic Circulation and Overturning (TRACOS; Schott et al., 2005), the SAMoc Basin-wide Array (SAMBA; Meinen et al., 2012), and the Rapid Climate Change–Meridional Overturning Circulation and Heatflux Array (RAPID–MOCHA; Cunningham et al., 2007), respectively. Repeated CTD lines are available at the latitudes of 24°N, 11°S, 24°S, 30°S, 32°S, and 34.5°S (Chidichimo et al., 2023). As a result, integrating information from fewer than ten transoceanic sections across the entire Atlantic basin poses fundamental challenges. Key questions remain regarding the connectivity between these isolated arrays: how do changes observed at one latitude relate to those detected elsewhere, what pathways link abyssal water masses between sections, and to what extent do observed signals reflect local processes versus basin-scale adjustments. Moreover, combining heterogeneous datasets from different observational initiatives, each with distinct sampling strategies and uncertainties, adds an additional layer of complexity. Together, these limitations hinder a comprehensive assessment of abyssal water mass pathways, variability, and basin-scale connectivity based solely on observations.

To overcome these observational limitations, numerical models and ocean reanalyses are widely used to complement *in situ* measurements and to provide a spatially and temporally continuous description of the ocean circulation. However, despite their widespread use, global ocean models and reanalyses exhibit important limitations in their representation of the abyssal ocean, which is often poorly resolved in state-of-the-art modeling systems. For example, Bailey et al. (2023) showed that the relatively coarse resolution of the Estimating the Circulation and Climate of the Ocean (ECCO), Simple Ocean Data Assimilation (SODA), and Southern Ocean State Estimate (SOSE) models does not realistically capture AABW formation, export, and variability in the Weddell Sea. Similarly, Heuzé (2020) argued that, although Climate Model Intercomparison

https://doi.org/10.5194/egusphere-2026-2319
Preprint. Discussion started: 5 May 2026

Project phase 6 (CMIP6) models exhibit substantial improvements compared to earlier generations, further developments are still required to correctly reproduce AABW formation rates, properties, and transports. Moreover, multi-model assessments such as the Ocean Model Intercomparison Project phase 2 (OMIP-2; Chassignet et al., 2020) have shown that increasing horizontal resolution alone does not necessarily improve the representation of deep-ocean thermohaline properties and may even degrade them in some regions, highlighting the need to better understand how resolution choices affect abyssal processes.

In this study, we focus on the western South Atlantic, a key region for the northward export of the AABW. We start by examining outputs from Estimating the Circulation and Climate of the Ocean (ECCO), Simple Ocean Data Assimilation (SODA), Global Ocean Physics Reanalysis (GLORYS), and the Ocean General Circulation Model for the Earth Simulator (OFES), to identify recurring strengths, limitations, and biases in their depiction of the abyssal characteristics. Motivated by indications that increasing horizontal resolution alone does not systematically improve deep-ocean simulations, we design a set of targeted numerical experiments using the Finite-Volume Sea Ice–Ocean Model (FESOM 2) to explore both the horizontal and vertical grid resolution influences on the representation of abyssal water properties and inter-basin connectivity. Resolutions are modified independently and in combination, while all other model components are kept unchanged, providing a controlled framework to assess their relative roles in shaping abyssal circulation in the western South Atlantic.

2 Data and numerical simulations

The present study analyzes three ocean reanalyses and five forward model simulations, four of which were specifically designed and conducted for this work. It also makes use of *in situ* data and climatological fields to support the evaluation of model performances.

2.1 *In situ* data

We used two *in situ* data sets. The first is a set of full-depth high-resolution Conductivity-Temperature-Depth (CTD) profiles of temperature from the trans-basin cruise aboard the R/V Maria S. Merian conducted in January 2017 (MSM60; Karstensen et al., 2019), and from thirteen years (2009-2022) of repeated cruises done in support to the maintenance of the western portion of the South Atlantic MOC Basin-wide Array (SAMBA-West), both along 34.5°S. We analyzed the longitudes of 48.5°W, 47.5°W, and 44.5°W. These sites correspond to the deployed locations of pressure-equipped inverted echo sounders (PIES) referred to as Sites BB, C, and D in the literature (Santos et al., 2025; Chidichimo et al., 2021; Valla et al., 2018), as illustrated in Fig. 1. For more information about the quality control and processing of the data, see Valla et al. (2018).

The second data set corresponds to three historic temperature time series sampled by sensors moored within the Vema Channel at nearby locations (Fig. 1). They were named as: “CLIVAR mooring” (Zenk, 2008); "E2 mooring" (Zenk and Visbeck, 2013); and "SAMBAR mooring" (Campos et al., 2021). The main information about each mooring is reported at Table 1.

https://doi.org/10.5194/egusphere-2026-2319
Preprint. Discussion started: 5 May 2026

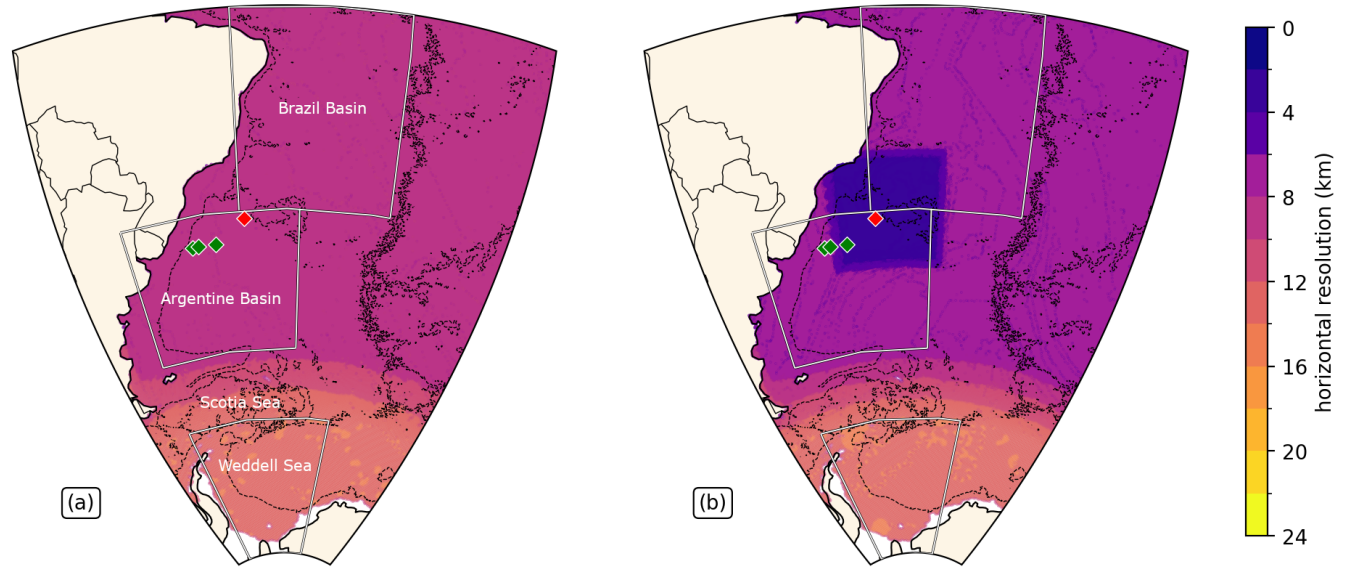

Figure 1. Panel a) Square root of grid-cell area (FESOM R and FESOM V) of the study region. Panel b) Same as panel a, but of FESOM H and FESOM VH. Green diamonds mark sites BB, C, and D and red diamond marks the approximate location of the three moorings within the Vema Channel. Highlighted areas represent, from north to south, the Brazil and Argentine basins and the Weddell Sea. Dashed black contour marks the isobath of 3000 m and solid black contour the continents.

Table 1. Summary of the mooring data sets used in this study.

Data set name	Location	Seafloor depth (m)	Sensor depth (m)	Pressure (bar)	Sampling period
CLIVAR	31.2383° S 39.3333° W	4580	4527	4612	12 Jan 1991 to 5 Dec 1992
E2	31.2547° S 39.3160° W	4544	4479	4557	31 May 2005 to 18 May 2007
SAMBAR	31.2333° S 39.3833° W	4630	4529	4610	1 Feb 2019 to 29 Aug 2019, 2020

2.2 World Ocean Atlas 2018 (WOA18)

The WOA18 climatology contains a set of long-term mean fields of ocean properties (Zweng et al., 2019; Locarnini et al., 2018). The data set consists of fields obtained through optimal interpolation of historic oceanographic data from different sources such as ship-deployed CTD, moored and drifting buoys, expendable bathythermographs (XBT), and gliders. The 0.25° annual climatological fields of temperature and salinity averaged between 1994 and 2005 were used for validation of the ocean simulation outputs. They were used to compute the σ_4 with the Thermodynamic Equation Of Seawater - 2010 software (TEOS-

https://doi.org/10.5194/egusphere-2026-2319
Preprint. Discussion started: 5 May 2026

10; IOC et al., 2010). We highlight that all comparisons with this data set were made utilizing its grid as reference, hence all model outputs were interpolated to match it.

2.3 Estimating the Circulation and Climate of the Ocean (ECCO)

We analyzed the outputs from the ECCO Version 4 release 4 (v4r4), its latest product release and the first to include the Arctic Ocean. This reanalysis is produced from the MIT General Circulation Model (MITgcm; Marshall et al., 1997). ECCO uses a unique grid formulation, in which between 70°S and 57°N a simple latitude-longitude (LL) grid is adopted, but out of this region a cubed-sphere grid (CS) is used; this configuration is known as the Lat-Lon-Cap (LLC) grid (Forget et al., 2015). Its horizontal resolution varies spatially from 22 km (high latitudes) to 110 km (mid-latitudes), and it has 50 vertical levels with different resolutions, varying from 10 m near the surface to 457 m between its two deepest levels. ECCO outputs are available from 1992 to 2017 with temporal resolution of hours, days, and months. The atmospheric forcing of this simulation is from the European Centre for Medium-Range Weather Forecasts interim reanalysis (ERA-Interim; Dee et al., 2011).

ECCO assimilates data from Argo floats, CTDs, XBTs, marine mammals, gliders, Ice-Tethered Profilers, moorings, and satellites (Fukumori et al., 2017). ECCO utilizes the adjoint method which simulates what is observed in the ocean based on the governing equations of motion (Forget et al., 2015; Thacker and Long, 1988), therefore the model conserves heat, salt, volume and momentum (Wunsch and Heimbach, 2007, 2013).

2.4 Simple Ocean Data Assimilation (SODA)

We used outputs from the SODA version 3.4.2m (Carton et al., 2018), downloaded from https://dsrs.atmos.umd.edu/DATA/soda3.4.2/REGRIDED/ocean/ on February 2, 2025. It is built on the Modular Ocean Model, version 5, ocean component of the Geophysical Fluid Dynamics Laboratory Coupled Model (GFDL CM2.5; Delworth et al., 2012). SODA's native horizontal grid is a tripolar Arakawa-B grid, which varies from 0.1°× 0.25° resolution at high latitude to 1/4°× 1/4° in the tropics, with 1440 × 1070 grid points. It has 50 vertical levels varying from 10 m resolution in the upper 100 m to much coarser resolution in the deep ocean. The atmospheric forcing of this simulation is from ERA-Interim (Dee et al., 2011). The product has an interpolated horizontal grid of 1/2° with 50 vertical levels, and it spans from 1980 to 2019 with a monthly resolution.

The main data sets that SODA assimilates are the World Ocean Database of historical hydrographic profiles (Boyer et al., 2013) and *in situ* and remotely sensed sea surface temperature. SODA assimilates data through the usage of an optimal interpolation method, in which the ocean state is constructed from a forecast based on the difference between the model and the observations (Carton et al., 2018).

2.5 Global Ocean Physics Reanalysis (GLORYS)

GLORYS is a global ocean and sea ice reanalysis product developed by the Mercator Ocean operational oceanography center. The version used in this study features a LL quasi-isotropic horizontal grid with a resolution of 1/12° and 50 vertical levels. The grid vertical spacing increases with depth, with resolution of 1 m near the surface and 450 m at 5000 m depth (Jean-

https://doi.org/10.5194/egusphere-2026-2319
Preprint. Discussion started: 5 May 2026

Michel et al., 2021). The simulation is conducted using the NEMO platform (Madec et al., 2008) and uses the fields from ERA-Interim as atmospheric forcing (Dee et al., 2011). The reanalysis spans the period from 1993 to 2018 at a monthly resolution and assimilates satellite-derived sea level anomaly, sea surface temperature, and sea ice concentration, along with *in situ* temperature and salinity vertical profiles, using a reduced-order Kalman filter.

2.6 Ocean General Circulation Model for the Earth Simulator (OFES)

We assessed OFES version 2 (Sasaki et al., 2020). This forward ocean model is based on version 3 of the Modular Ocean Model (MOM) (Pacanowski and Griffies, 1999) and runs on a LL grid system. It has a horizontal resolution of 0.1°, spanning the global ocean from 76°S to 76°N. A sea-ice component (Komori et al., 2005) is incorporated to simulate conditions in the Antarctic and subarctic seas. Atmospheric forcing is provided by the JRA-55 reanalysis data set (Kobayashi et al., 2015), with the simulation covering the period 1958 to 2016 (Sasaki et al., 2020). The model focuses on the upper ocean, with a vertical resolution of 5 m in the top 100 m. Of the 105 total vertical levels, 55 lie within the upper 500 m, and the remaining 50 span depths from 500 m to 7500 m. The top 21 levels are uniformly spaced at 5 m, while the deepest six have 300 m intervals.

2.7 FESOM 2 simulations

The Finite-Element Sea Ice–Ocean Model (FESOM) (Wang et al., 2014) is the first fully developed global multi-resolution model specifically designed to simulate large-scale ocean dynamics. Its next-generation counterpart, the Finite-volumE Sea ice–Ocean Model (FESOM 2), adopts a finite-volume discretization approach in place of the finite-element discretization used in the original model. This shift significantly enhances efficiency, making FESOM 2 at least nine times faster than its predecessor (Danilov et al., 2017).

FESOM 2 utilizes a horizontal triangular mesh with horizontal velocity components defined at the centers of the triangles, while scalar variables are positioned at its vertices. The vertical grid adopts the Lagrangian-Eulerian (ALE) vertical coordinate system (Donea and Huerta, 2003), with both horizontal velocities and scalar variables defined between vertical levels, whereas inter-layer exchange velocities are located at the layer interfaces and aligned with scalar positions. FESOM 2 contains a sea-ice component that has been derived from the Finite-Element Sea Ice Model (FESIM) (Danilov et al., 2015).

The simulations use a default model configuration in which each experiment is forced with the JRA55 atmospheric reanalysis, initialized from the Polar Science Center Hydrographic Climatology (PHC; Steele et al. 2001). We use the Gent-McWilliams eddy parameterization (Gent and Mcwilliams, 1990) and the Redi (1982) isoneutral diffusion. Diffusivity is scaled linearly with resolution, with a reference diffusivity of 2000 m^2s^{-1} at 100 km horizontal resolution. As the vertical mixing scheme, we employ the K-profile parameterization (KPP; Large et al. 1994). No additional calibration was applied to tailor the model to specific regions or processes of interest.

The first simulation, hereafter referred to as FESOM R (from reference) was designed to replicate results from existing numerical simulations, such as ECCO, SODA, OFES, and GLORYS. To achieve this, we adopted the exact vertical levels used in OFES, as it includes the highest number of vertical levels among the evaluated simulations. Hence, FESOM R employs 105 vertical levels that extend from the surface to 7350 dbar, with five levels distributed between 3800 dbar and 5350 dbar. The

https://doi.org/10.5194/egusphere-2026-2319
Preprint. Discussion started: 5 May 2026

base horizontal resolution was set to 30 km, with coarser resolution in the North Pacific and Indian oceans (110 km) and finer resolution in the South Atlantic Ocean (10 km) (Fig. 1a; Fig. S1a).

The second simulation, hereafter referred to as FESOM V (from vertical) was designed to evaluate the impact of vertical resolution. It retains all configurations of FESOM R but increases the number of vertical levels, particularly near the ocean bottom. FESOM V employs 125 vertical levels extending from the surface down to 5350 dbar, with additional levels concentrated between 3800 dbar and 5350 dbar. This configuration provides a vertical resolution of approximately 50 m near the seafloor, resulting in 31 vertical levels within this range. Above 3800 dbar, FESOM V shares the same vertical level structure as FESOM R.

The third simulation, hereafter referred to as FESOM H (from horizontal), was designed to evaluate the impact of horizontal resolution. This experiment retains all configurations of FESOM R, but increases the horizontal resolution in key regions relevant to the northward flow of abyssal waters in the Atlantic Ocean, with FESOM H maintaining the original 105 vertical levels while increasing the horizontal resolution in the South Atlantic sector to 7.5 km and further refining it to 4 km in the Vema Channel and its surrounding area (Fig. 1b and S1b).

The fourth simulation, hereafter referred to as FESOM VH, was designed to evaluate how the two previous configurations work together. FESOM VH enhances both vertical and horizontal resolution. This experiment uses the same vertical resolution as FESOM V and the same horizontal resolution as FESOM H. The main characteristics of the numerical simulations are reported in Table 2.

Table 2. Summary of the main characteristics of the ocean numerical simulations evaluated in this study. The pressure range (3800–6000) is given in dbar.

System	Model	Grid	Resolution	Layers (3800–6000)	Forcing	Assimilation method	Period
ECCO	MITgcm	LLC	110–22 km (50 lev.)	4	ERA-Interim	Adjoint	1992-2017
SODA	GFDL CM2.5	Arakawa-B	1/4°–1/10° (50 lev.)	8	ERA-Interim	Optimal Interpolation	1980-2019
GLORYS	NEMO	LL	1/12° (50 lev.)	4	ERA-Interim	Reduced-order Kalman	1993-2018
OFES	MOM	LL	1/10° (105 lev.)	5	JRA55	-	1958-2016
FESOM R	FESOM 2	Triangular	110–10 km (105 lev.)	5	JRA55	-	1958-2020
FESOM V	FESOM 2	Triangular	110–10 km (125 lev.)	31	JRA55	-	1958-2020
FESOM H	FESOM 2	Triangular	110–4 km (105 lev.)	5	JRA55	-	1958-2020
FESOM VH	FESOM 2	Triangular	110–4 km (125 lev.)	31	JRA55	-	1958-2020

3 ECCO, SODA, GLORYS, and OFES results

In the following section, we first evaluate the representation of abyssal water masses in ECCO, SODA, GLORYS, and OFES by comparing model outputs with *in situ* observations and WOA18 climatology. This analysis allows us to quantify both common and model-specific biases and to identify key deficiencies in the simulated abyssal representation.

https://doi.org/10.5194/egusphere-2026-2319
Preprint. Discussion started: 5 May 2026

3.1 Abyssal properties

We constructed horizontal maps of abyssal water properties (θ, salinity, and σ_4), covering the Antarctic continental shelf and slope, the central Weddell Sea, and the western South Atlantic. The latter includes the Argentine and Brazil basins, defined as follows: the Argentine Basin spans 50°S–30°S and 60°W–30°W, while the Brazil Basin extends from 30°S to 0° and from 40°W to 15°W (Fig. 1, white boxes). Data were extracted from the deepest valid level at each horizontal grid point over the same period as the WOA18 dataset (1994–2005) at monthly resolution. For each simulation, we calculated the time-averaged field and the mean bias (simulation minus reference).

The reference θ field (Fig. 2a) shows cold abyssal waters below -0.7°C on the Antarctic continental shelf (Fig. 2, white contours), characteristic of DSW. Along the continental slope, temperatures increase, forming a band of relatively warmer water that separates the shelf from the central abyssal Weddell Sea. This feature likely reflects the limited horizontal and vertical resolution of WOA18, as the dense shelf water plume cascading downslope to form WSDW and WSBW is relatively narrow and thin and may not be fully resolved, being smoothed by spatial averaging. In the central Weddell Sea, temperatures drop below -0.7°C again, indicating the presence of WSBW, which does not penetrate into the Scotia Sea, where higher temperatures prevail due to the presence of WSDW only (Fig. 2, red contours). In the Argentine Basin, waters with $\theta \leq 0$°C are observed, corresponding to AABW, which enters the Brazil Basin through the Vema Channel and progressively modifies its properties as it flows northward.

ECCO, SODA, GLORYS, and OFES all depict cold waters ($\theta < -0.7$°C) over the Antarctic continental shelf (Fig. 2b, c, d, and e). In the central Weddell Sea, ECCO, GLORYS, and OFES also reproduce waters colder than -0.7°C, although the cold region in ECCO is spatially limited. SODA is the only product that fails to reproduce this feature, with central Weddell Sea bottom temperatures of approximately -0.35°C. OFES, at the other extreme, depicts waters colder than -1.4°C.

The northward spreading of cold waters from the Weddell Sea is limited in ECCO, SODA, and GLORYS (Fig. 2b, c, and d). OFES (Fig. 2e) is the only product that reproduces the presence of WSBW in the South Sandwich Trench, a deep channel located east of the South Scotia Ridge, and of WSDW in the Scotia Sea. ECCO, GLORYS, and OFES capture cold waters with -0.7°C $< \theta < 0.0$°C in the Argentine Basin, but only OFES represents their further northward spreading through the Vema Channel into the Brazil Basin. SODA again stands out as an exception, with relatively warm waters in both the Argentine and Brazil Basins.

The results above describe the spatial extent of cold waters exported from the Weddell Sea. However, the bias fields reveal important regional contrasts throughout the study area. Despite the persistence of cold waters along the continental shelf, all simulations exhibit positive temperature biases, particularly along the eastern sector of the southern continental shelf (Fig. 2f, g, h, and i). In contrast, the eastern shelf of the Antarctic Peninsula, located to the west of this region, shows negative temperature biases, with the exception of ECCO, which exhibits a warm bias. In the abyssal central Weddell Sea (depths > 3000 m), ECCO, SODA, and GLORYS are warmer than the reference, whereas OFES shows colder values.

In the Argentine Basin, abyssal waters are warmer than the reference in SODA and OFES. GLORYS exhibits localized colder patches in the southern and northwestern portions of the basin and warmer regions surrounding these patches. ECCO,

https://doi.org/10.5194/egusphere-2026-2319
Preprint. Discussion started: 5 May 2026

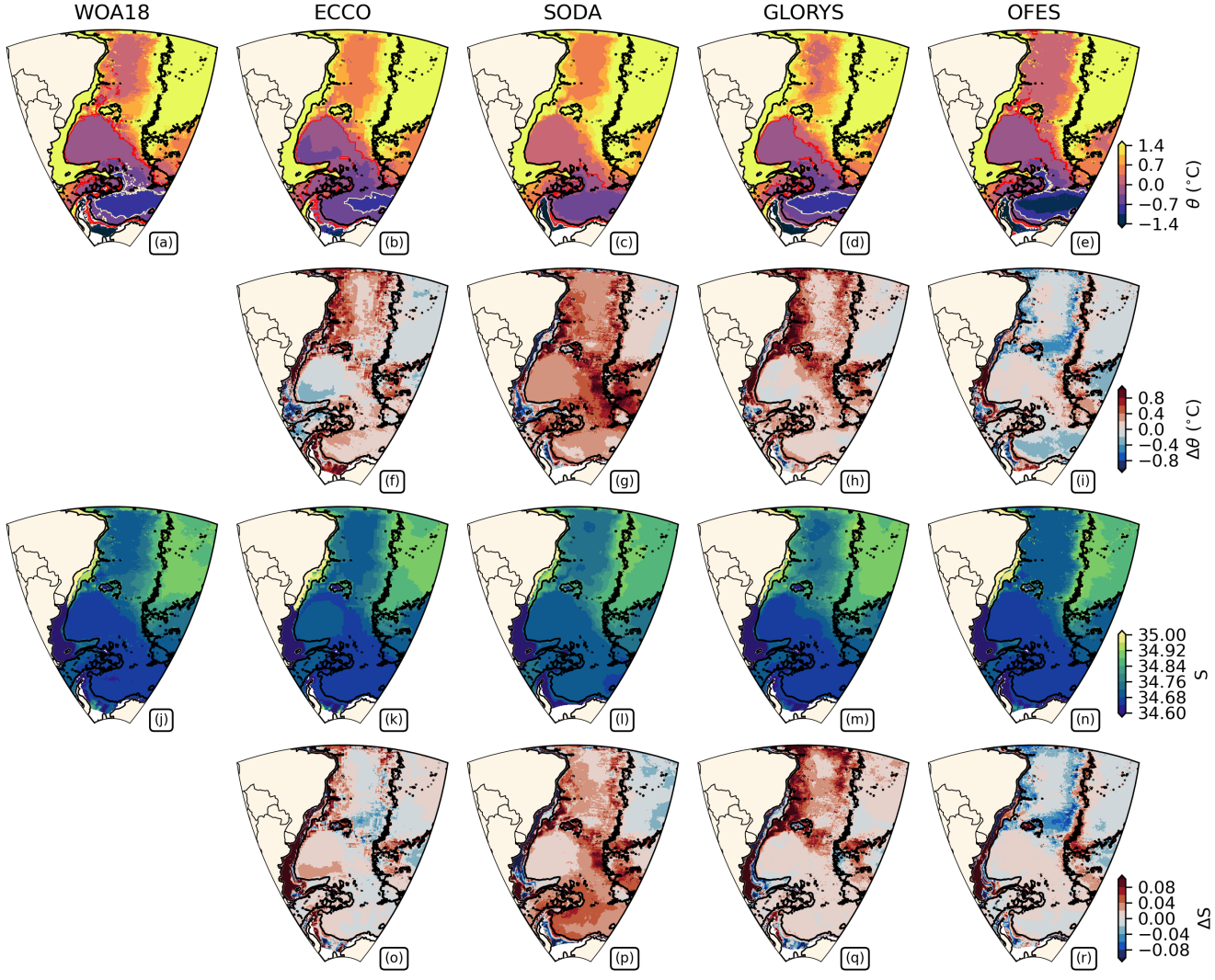

Figure 2. Total mean potential temperature (θ; panels a–e) and salinity (panels j–n) from 1994 to 2005 at the deepest valid level at each horizontal grid point, and the corresponding mean biases relative to WOA18 ($\Delta\theta$, panels f–i; ΔS, panels o–r). Columns correspond to WOA18 (reference), ECCO, SODA, GLORYS, and OFES, from left to right. The black contour indicates the 3000 m isobath, the red contour marks the $\theta = 0.0°$C isotherm, and the white contour marks the $\theta = -0.7°$C isotherm.

by contrast, shows a consistent cold bias throughout this basin. In the Brazil Basin, ECCO, SODA, and GLORYS depict warmer conditions than the reference, while OFES shows a mixture of warm and cold regions, with the negative bias dominating over a larger portion of the basin. Notably, ECCO and OFES, the former more strongly, the latter more subtly, exhibit opposite bias signs between the Weddell Sea, the Argentine Basin, and the Brazil Basin, whereas SODA and GLORYS show consistently warm conditions across all three regions.

https://doi.org/10.5194/egusphere-2026-2319
Preprint. Discussion started: 5 May 2026

The reference salinity field (Fig. 2j) displays alternating regions of relatively high (> 34.84) and low (< 34.68) salinity on the continental shelf. In the central Weddell Sea, bottom salinities are approximately 34.68, and these values persist northward through the Argentine Basin. Within the Brazil Basin, salinity increases from approximately 34.72 in the basin interior to 34.88 near its boundaries.

ECCO, GLORYS, and OFES correctly reproduce the alternating salinity bands on the Antarctic continental shelf (Fig. 2k, m, and n), whereas SODA does not cover this region (Fig. 2l). In the central Weddell Sea, ECCO, GLORYS, and OFES depict salinities near 34.68, while SODA shows comparatively higher values. In the Argentine Basin, GLORYS and OFES also reproduce salinities near 34.68, although GLORYS exhibits saltier waters in the northeastern portion of the basin. ECCO displays the opposite pattern, with saltier waters in the central basin and fresher values toward its margins, while SODA shows the highest salinities of all products throughout the basin. In the Brazil Basin, SODA and GLORYS depict the saltiest conditions, OFES shows the freshest waters, and ECCO exhibits intermediate salinity values.

ECCO, GLORYS, and OFES generally exhibit positive salinity anomalies along the eastern side of the Antarctic Peninsula and fresh biases farther east on the Antarctic continental shelf, near the southern limit of each model domain (Fig. 2o, q, r). SODA, in contrast, shows a consistent fresh bias across these regions (Fig. 2p). In the central Weddell Sea, SODA and GLORYS display predominantly salty biases, with SODA presenting the largest deviations, while ECCO and OFES exhibit a mixture of positive and negative anomalies. In the Argentine Basin, all four products depict saltier-than-reference conditions. This signal extends into the Brazil Basin for ECCO (with some localized negative patches), SODA, and GLORYS, whereas OFES stands out by exhibiting predominantly negative anomalies across most of the basin, resulting in a marked basin-to-basin contrast, with fresher conditions in the Weddell and Brazil Basins and saltier waters in the Argentine Basin.

The reference σ_4 field (Fig. S2a) shows high-density waters ($\sigma_4 > 46.3$ kg m^{-3}) over the Antarctic continental shelf. In the central Weddell Sea, bottom densities are slightly lower ($\sigma_4 \approx 46.2$ kg m^{-3}) and extend toward the Scotia Ridge without crossing it, as well as eastward into the South Sandwich Trench. In the Argentine Basin, lighter bottom waters are found ($\sigma_4 \approx 46.1$ kg m^{-3}). Farther north, these waters leak through the Vema Channel into the Brazil Basin, where densities decrease slightly as they progress northward ($\sigma_4 \approx 46.04$ kg m^{-3}). The spatial patterns described for θ are largely mirrored in the σ_4 field (Fig. S4, first row). As a consequence, the latter displays positive (negative) biases where the former shows negative (positive) anomalies, indicating that density variations are primarily controlled by temperature rather than salinity in these simulations.

Dense and cold waters are present along the Antarctic continental slope in all simulations. However, none of them show clear evidence of DSW plumes cascading downslope to form new WSBW and WSDW (see supplementary videos). In ECCO, the central Weddell Sea is initially occupied by relatively light waters that gradually become denser over time. SODA shows episodic pulses of denser waters in this region, and the basin as a whole becomes denser by the end of the simulation relative to its initial state, with periods of rapid water mass transformation also occurring. GLORYS, in contrast, exhibits comparatively little temporal variability. However, because its outputs are not continuous in time, the temporal evolution appears as intermittent pulses rather than a smooth progression, as seen in the supplementary animation. OFES starts with very dense abyssal waters that gradually become lighter over time, yet remain denser than those in the other products throughout the simulation.

https://doi.org/10.5194/egusphere-2026-2319
Preprint. Discussion started: 5 May 2026

In the Argentine and Brazil Basins, the simulations also exhibit distinct temporal evolutions. In ECCO, SODA, and OFES, the long-term trends in these basins differ from those observed in the Weddell Sea. While the Weddell Sea tends to become denser over time in ECCO and SODA, the Argentine and Brazil Basins show a general lightening trend. OFES presents a similar inter-basin contrast but with the opposite sign: the Argentine and Brazil Basins show an initial increase in density followed by a gradual decrease, yet abyssal waters remain denser at the end of the simulation than at the beginning. This contrast between the Weddell Sea and the adjacent basins in ECCO, SODA, and OFES may indicate limitations in the representation of deep-basin connectivity. GLORYS, in contrast, shows relatively small temporal changes and a similar pattern across all three basins, although the lack of temporal continuity in its outputs complicates the interpretation of its variability.

Overall, the comparison of θ, salinity, and σ_4 shows that all simulations broadly capture the large-scale distribution of abyssal water masses, but exhibit consistent limitations in their representation of abyssal properties and inter-basin connectivity. ECCO and OFES reproduce the general thermohaline structure but display contrasting bias patterns between basins, while SODA shows a more spatially uniform yet persistently warm and saline deep ocean. Across all simulations, density biases closely follow temperature errors, indicating that inaccuracies in the θ field are the primary driver of the discrepancies in the σ_4 field. Moreover, none of the simulations clearly represents dense shelf water cascading from the Antarctic continental shelf, and the inconsistent temporal evolution of abyssal density between the Weddell Sea and the Argentine and Brazil Basins further points to limitations in the representation of deep-basin connectivity.

3.2 TS diagram analysis

To further examine the discontinuities between connected basins, we focus on the Argentine and Brazil basins. While the pathways connecting the Southern Ocean to the Argentine Basin involve complex topographic features such as the Scotia Ridge and multiple fracture zones, the Vema Channel provides a relatively direct and well-defined passage linking the Argentine and Brazil basins. We therefore analyze the θ–S relationship in each simulation and compare it with the corresponding reference (Fig. 3a and b).

In the Argentine Basin, ECCO exhibits a noticeable scattered dispersion of waters lighter than 45.84 kg m^{-3} and a tilt of the curve toward higher salinity values at densities above 45.92 kg m^{-3} (Fig. 3c), while SODA presents a shape closer to the reference, though lacking waters colder than 0.0°C (Fig. 3g). Despite these differences, both simulations share a common limitation when transitioning to the Brazil Basin: the θ–S distribution shows a marked reduction in the occurrence of the densest water classes and a systematic shift of the entire curve toward lighter densities relative to the reference (Fig. 3e, f, i, and j), indicating a discontinuity in abyssal water transport through the Vema Channel.

GLORYS closely follows the reference θ–S curve in the Argentine Basin, including waters colder than 0.0°C and with only minor deviations from the reference (Fig. 3k and l). OFES presents a similar overall shape but with a narrower salinity range (Fig. 3o and p). In the Brazil Basin, GLORYS shows a striking reduction in the number of θ–S occurrences for the density range of 45.84–45.92 kg m^{-3} (Fig. 3m), indicating a lack of the densest bottom water masses, though the overall shape of the curve still agrees with the reference (Fig. 3n). OFES, in contrast, exhibits a shift of the entire curve toward lighter densities, similar to ECCO and SODA, but retains slightly denser waters at the very bottom of the basin (Fig. 3q and r).

https://doi.org/10.5194/egusphere-2026-2319
Preprint. Discussion started: 5 May 2026

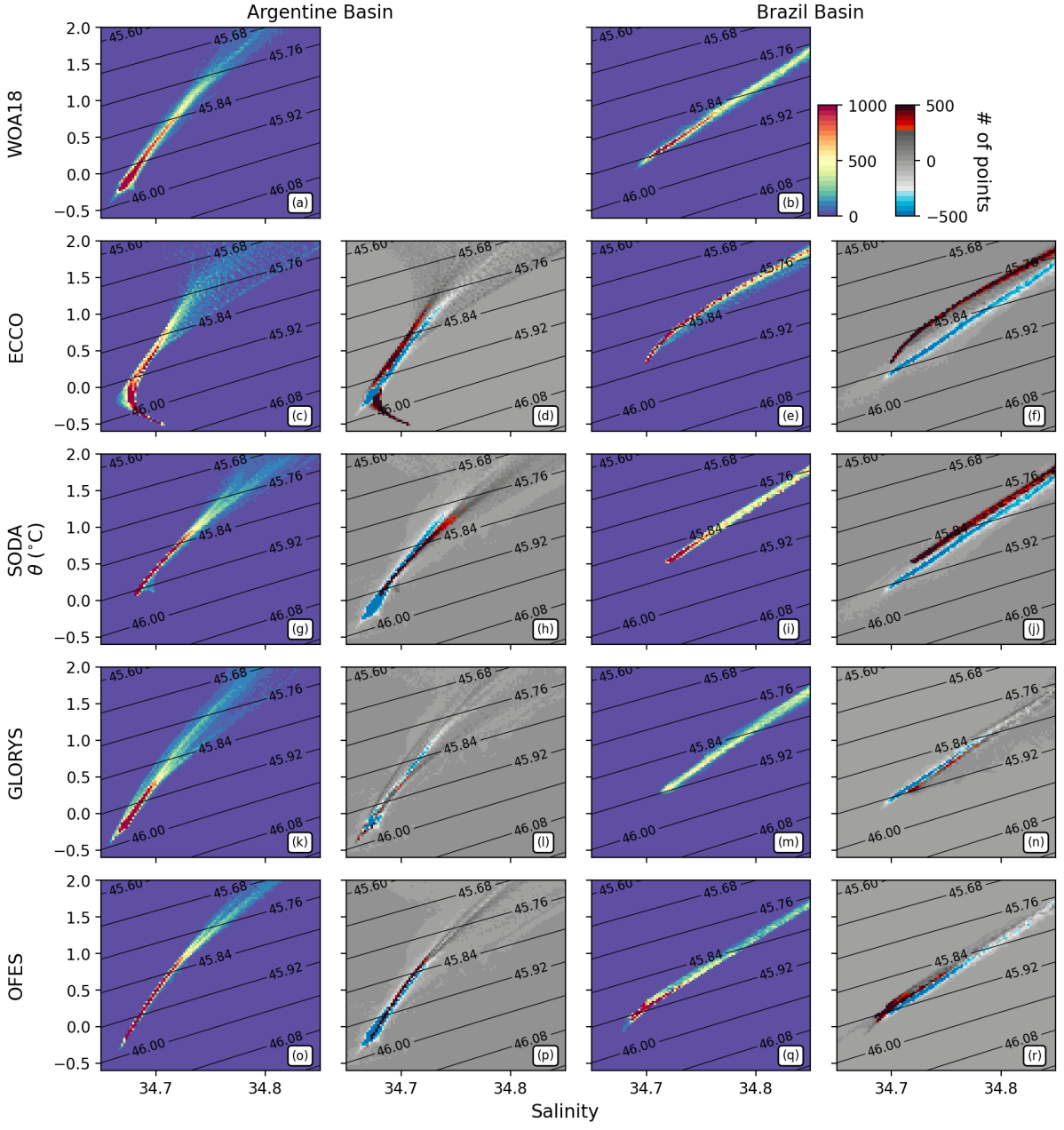

Figure 3. Time averaged θ–S distribution of the Argentine Basin (first column) and of the Brazil Basin (third column). Averaged θ–S distribution of the difference between WOA18 and each simulation at the Argentine Basin (second column) and at the Brazil Basin (fourth column). The rows from top to bottom represent WOA18 (first row), ECCO (second row), SODA (third row), GLORYS (fourth row), and OFES (fifth row). Contour lines are σ_4. The diagrams are zoomed to the abyssal layer ($-0.6^\circ\mathrm{C} < \theta < 2.0^\circ\mathrm{C}$; $34.65 < S < 34.85$).

https://doi.org/10.5194/egusphere-2026-2319
Preprint. Discussion started: 5 May 2026

The θ–S analysis reveals that, while the simulations differ in how they represent abyssal water properties in the Argentine Basin, they all exhibit a common discontinuity when transitioning to the Brazil Basin. The way this discontinuity manifests, however, differs between products: ECCO, SODA, and OFES show a systematic shift of the entire θ–S curve toward lighter densities, whereas GLORYS shows a volumetric reduction concentrated in the densest water classes while broadly preserving the overall shape of the curve. Together, these results point to a limitation in the representation of abyssal water mass connectivity across the Vema Channel.

3.3 Temperature distribution across Vema Channel

The differences identified in the θ–S characteristics between the Argentine and Brazil basins indicate discontinuities in abyssal water properties along the northward pathway. To better understand where and how these discontinuities develop, we next focus on the Vema Channel, the main passage connecting the two basins. Examining the temperature structure within this region provides a direct way to assess how deep-water masses are represented as they flow from the Argentine to the Brazil Basin.

The WOA18 reference field reveals a discrepancy between the actual location of the Vema Channel and its representation (Fig. 4a). Only three vertical levels cover the channel, spanning a total of five grid points, none of which capture its full depth. Despite this, the reference field indicates the presence of waters colder than 0.0°C in the region corresponding to the channel, suggesting that WOA18 captures at least the thermal signature of the abyssal flow, even if its spatial structure remains poorly resolved.

The Vema Channel is absent in both ECCO (Fig. 4b) and SODA (Fig. 4c). In ECCO, a single column of grid points is present in the region where the channel should be located, whereas the SODA grid contains no points in this region, despite being slightly deeper. In both simulations, the temperature section shows waters warmer than the reference with no waters colder than 0.0°C. GLORYS provides a better representation of the channel (Fig. 4d), with two vertical levels inside it: the deepest containing two grid points approximately 300 m above the actual bottom, and the shallower containing four. Nevertheless, no waters colder than 0.0°C are found within the channel. In OFES, the channel structure is slightly misaligned with its actual location (Fig. 4e). The number of grid points and vertical levels inside the channel matches those in GLORYS, but the abyssal waters are colder and less stratified than the reference.

In the region of the Vema Channel, ECCO, SODA, and GLORYS all exhibit positive temperature biases relative to the reference, while OFES is colder. For SODA and GLORYS, this is consistent with the warm bias observed throughout the Argentine Basin (Fig. 2g and h). In ECCO, however, this represents an inversion of the pattern seen in the Argentine Basin, where waters are significantly colder than the reference (Fig. 2f), pointing to a lack of connectivity between the two basins, with the coldest waters of the Argentine Basin likely remaining trapped there due to the absence of sufficiently deep vertical levels. OFES, in turn, shows a counterintuitive inversion in the opposite direction, shifting from a warm bias in the Argentine Basin to a cold bias within the Vema Channel and into the Brazil Basin.

https://doi.org/10.5194/egusphere-2026-2319
Preprint. Discussion started: 5 May 2026

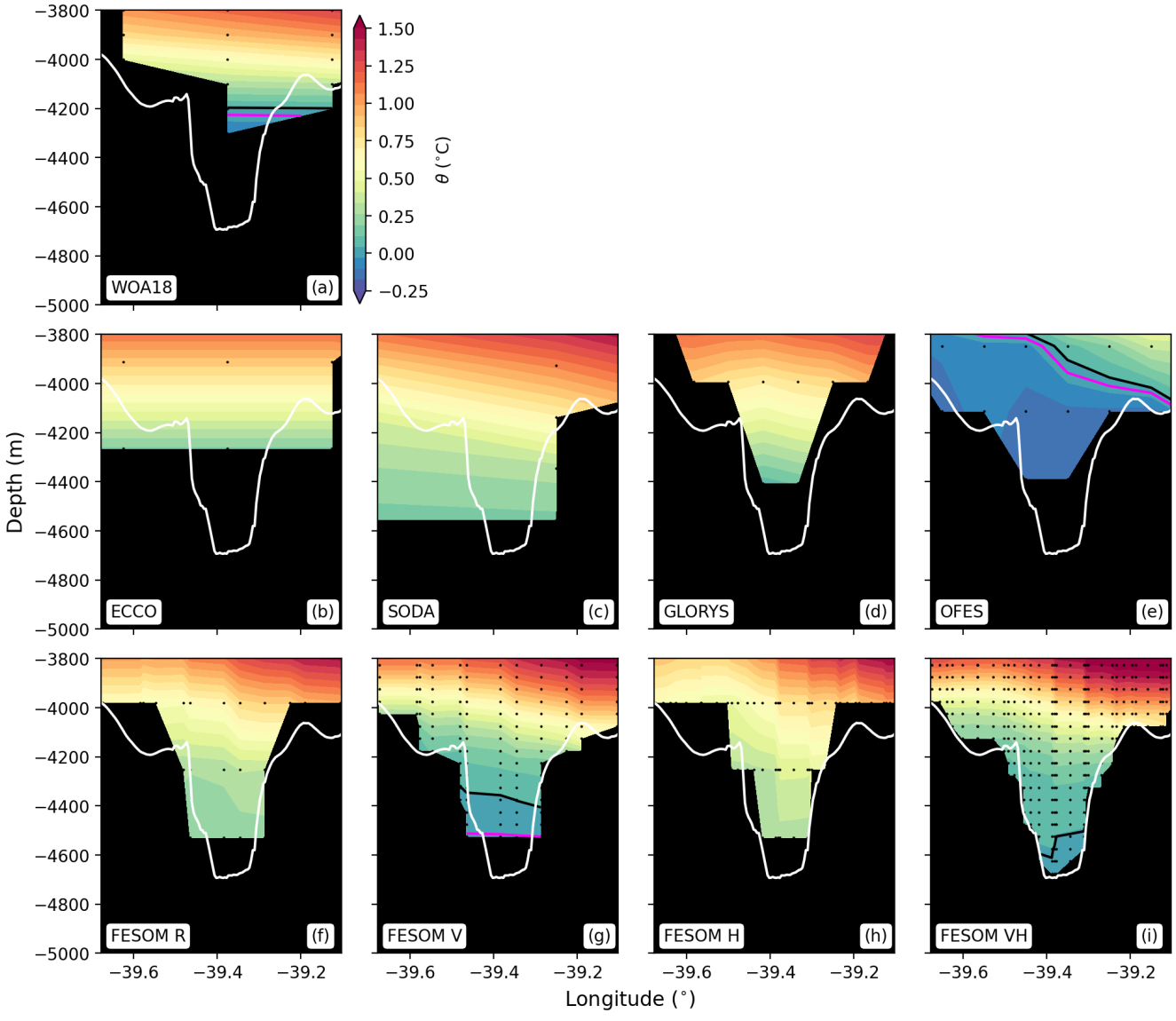

Figure 4. Time-averaged potential temperature (θ) from 1995 to 2004 across Vema Channel at 31.3°S from: WOA18 (a), ECCO (b), SODA (c), GLORYS (d), OFES (e), FESOM R (f), FESOM V (g), FESOM H (h), and FESOM VH (i). Black dots are the grid points, white line is the bathymetry from the General Bathymetric Chart of the Oceans (GEBCO), black line is the isotherm of 0.04°C, and magenta line is the isotherm of 0.00°C.

3.4 Comparison with *in situ* data

Here we compare simulation outputs with *in situ* observations from three moorings deployed within the Vema Channel (Table 1). Comparing OGCM outputs against pointwise *in situ* observations is an inherently demanding test, given that OGCMs are

https://doi.org/10.5194/egusphere-2026-2319
Preprint. Discussion started: 5 May 2026

not designed to resolve variability at these small scales. Accordingly, this analysis should not be interpreted as a conventional validation, but rather as an exploration of model performance under such unfavorable conditions.

During the CLIVAR period, ECCO shows the highest correlation among the four products but its mean temperature substantially deviates from the reference (Fig. 5a and d). SODA shows a weaker correlation and a similarly large deviation from the reference mean. GLORYS achieves a moderate correlation but with considerably larger variability (Fig. S3a), while its mean temperature is closer to the reference than ECCO and SODA. OFES exhibits a slightly negative correlation but provides the closest representation of the reference mean among the four products.

During the E2 period, ECCO shows an improved correlation relative to the CLIVAR period, but with increased variability, and its mean temperature remains similar to CLIVAR though slightly warmer than the reference (Fig. 5b and e). SODA exhibits a more negative correlation and larger variability than in CLIVAR, with a mean temperature that deviates more from the reference. GLORYS shows a reduced correlation and increased variability relative to CLIVAR (Fig. S3b), but its mean temperature remains closer to the reference than ECCO and SODA. OFES exhibits a more negative correlation than in CLIVAR but improved variability, and again provides the closest representation of the reference mean among the four products.

During the SAMBA period, only SODA and GLORYS provide outputs. SODA shows a small but positive correlation and statistical metrics similar to the CLIVAR period, but its mean temperature deviates even further from the reference, suggesting a possible overestimation of the abyssal ocean warming trend (Santos et al., 2025; Johnson, 2022). GLORYS shows a correlation similar to the CLIVAR period, but its variability remains excessive (Fig. S3c). Unlike SODA, GLORYS does not exhibit a pronounced warming trend.

In addition to the mooring records, the simulations were compared with CTD data from the SAMBA-West array, just south of the Vema Channel at Sites BB, C, and D (Fig. 1, green diamonds). We used the deepest bin of each CTD cast to construct the reference time series, shown as black stars in Fig. 6. Mean temperatures and linear trends for each simulation and site are summarized in Table 3.

At Site BB, all simulations produce temperatures warmer than the reference (Fig. 6a, Table 3). OFES is the only simulation with a mean temperature close to the reference, though still slightly warmer, whereas ECCO, SODA, and GLORYS substantially overestimate it, with GLORYS additionally exhibiting the largest uncertainty among the four products. The observed CTD trend at this site is not statistically significant, which excludes a meaningful comparison of warming trends with the simulations.

At Site C, ECCO and SODA overestimate the reference mean temperature, with SODA showing the largest deviation (Fig. 6b, Table 3). GLORYS is slightly below the reference while OFES is slightly above, both with the same absolute deviation, though GLORYS exhibits considerably larger uncertainty. Regarding trends, ECCO provides the closest match to the observed warming trend, while SODA substantially overestimates it. GLORYS shows a cooling trend in contrast to the observed warming, and OFES overestimates it moderately. Overall, OFES provides the best representation of the reference mean, while ECCO captures the observed trend most accurately.

At Site D, SODA again shows the largest deviation from the reference mean, while OFES provides the closest representation with a mean temperature only slightly above the reference (Fig. 6c, Table 3). Notably, ECCO shifts from overestimating the

https://doi.org/10.5194/egusphere-2026-2319
Preprint. Discussion started: 5 May 2026

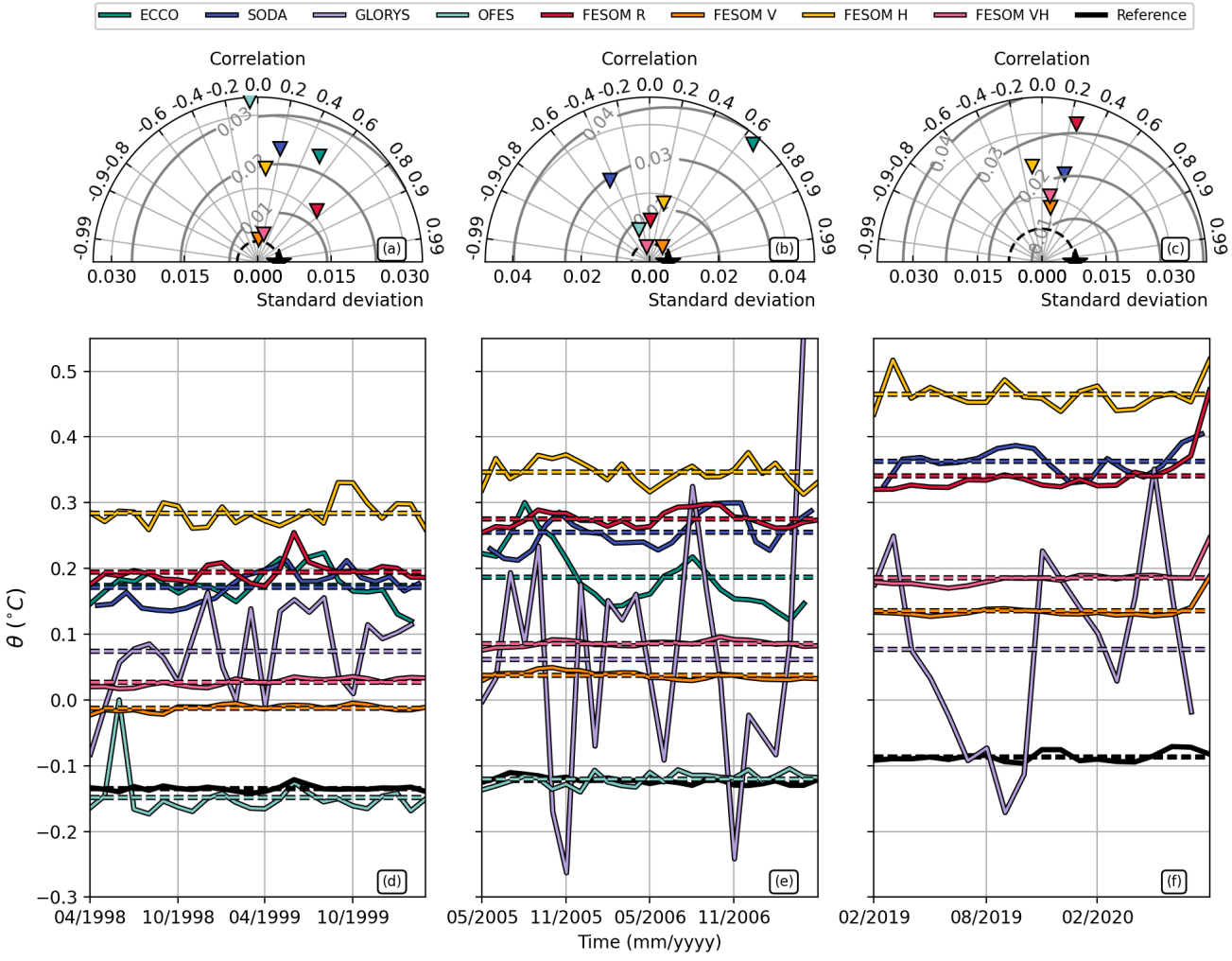

Figure 5. Taylor diagrams comparing simulation outputs with *in situ* temperature records from sensors moored within the Vema Channel (top row), and the corresponding temperature time series (bottom row). Dashed lines indicate the mean temperature for each dataset. Columns correspond to the CLIVAR (left), E2 (center), and SAMBA (right) mooring periods. The reference (black) corresponds to the mooring measurements. Colors indicate: ECCO (green), SODA (dark blue), GLORYS (lavender), OFES (light green), FESOM R (red), FESOM V (orange), FESOM H (yellow), and FESOM VH (pink).

reference mean at Sites BB and C to underestimating it here, highlighting spatial variations in its performance. GLORYS remains close to the reference mean but with large uncertainty. Regarding trends, ECCO again provides the closest match to the observed warming trend, while SODA substantially overestimates it. GLORYS shows a near-zero trend, and OFES moderately overestimates it.

https://doi.org/10.5194/egusphere-2026-2319
Preprint. Discussion started: 5 May 2026

Table 3. Mean temperature and linear trend from simulation outputs and CTD observations (reference) at Sites BB, C, and D along the SAMBA-West array. The reference corresponds to the deepest bin of each CTD cast. Trends are computed over the same period as the CTD observations at each site. Trend values are multiplied by 10^3 for display purposes.

	Site BB		Site C		Site D	
	Mean (°C)	Trend (10^{-3} °C yr^{-1})	Mean (°C)	Trend (10^{-3} °C yr^{-1})	Mean (°C)	Trend (10^{-3} °C yr^{-1})
Reference	-0.10 ± 0.02	-0.8 ± 2.7	-0.12 ± 0.007	2.1 ± 1.2	-0.13 ± 0.008	1.9 ± 1.1
ECCO	0.54 ± 0.01	2.2 ± 0.2	0.09 ± 0.008	1.4 ± 0.1	-0.17 ± 0.003	0.5 ± 0.1
SODA	0.40 ± 0.05	7.6 ± 0.7	0.31 ± 0.03	6.9 ± 0.4	0.26 ± 0.027	7.6 ± 0.4
GLORYS	0.29 ± 0.24	-10.0 ± 3.2	-0.14 ± 0.10	-4.2 ± 1.4	-0.08 ± 0.080	-0.1 ± 1.0
OFES	-0.05 ± 0.04	4.4 ± 0.9	-0.10 ± 0.009	3.0 ± 0.2	-0.11 ± 0.009	3.8 ± 0.2
FESOM R	0.71 ± 0.05	1.5 ± 0.6	0.30 ± 0.026	5.6 ± 0.4	0.25 ± 0.02	4.9 ± 0.3
FESOM V	0.19 ± 0.05	9.7 ± 0.6	0.09 ± 0.02	5.6 ± 0.3	0.07 ± 0.02	6.3 ± 0.3
FESOM H	0.62 ± 0.05	2.5 ± 0.6	0.36 ± 0.03	7.6 ± 0.4	0.33 ± 0.03	8.1 ± 0.4
FESOM VH	0.25 ± 0.04	8.2 ± 0.5	0.15 ± 0.024	6.8 ± 0.3	0.12 ± 0.02	6.9 ± 0.3

In summary, the comparison highlights that model performance varies substantially across locations and periods, with no single simulation consistently outperforming the others. SODA consistently overestimates the reference mean temperature across all sites, while GLORYS, despite reproducing mean conditions reasonably well, exhibits excessive variability throughout. OFES generally provides the closest representation of the observed mean temperature, and ECCO captures the warming trends most accurately, though with notable spatial variations in its mean temperature performance. Together, these results reinforce the limitations identified in the previous sections regarding the representation of abyssal water properties in the western South Atlantic.

4 FESOM results

While ECCO, SODA, GLORYS, and OFES broadly capture the large-scale distribution of abyssal water masses, they exhibit consistent limitations in the representation of abyssal properties and inter-basin connectivity, with no clear indication of their origins. To investigate the role of grid resolution in driving these limitations, we designed four targeted experiments using FESOM 2, in which horizontal and vertical resolution are modified independently and in combination, while all other model components are kept unchanged.

4.1 Abyssal properties

The bottom temperature distribution in FESOM R (Fig. 7b) exhibits several features similar to those in the previous simulations. Cold waters ($\theta < -0.7$°C) are present over the Antarctic continental shelf, a pattern common to all four FESOM simulations. As in ECCO (Fig. 2b), only a limited area of the central Weddell Sea is occupied by waters colder than -0.7°C. Waters with $\theta \leq 0.0$°C extend northward into the Argentine Basin but remain confined to its southern portion, leading to the predominance

https://doi.org/10.5194/egusphere-2026-2319
Preprint. Discussion started: 5 May 2026

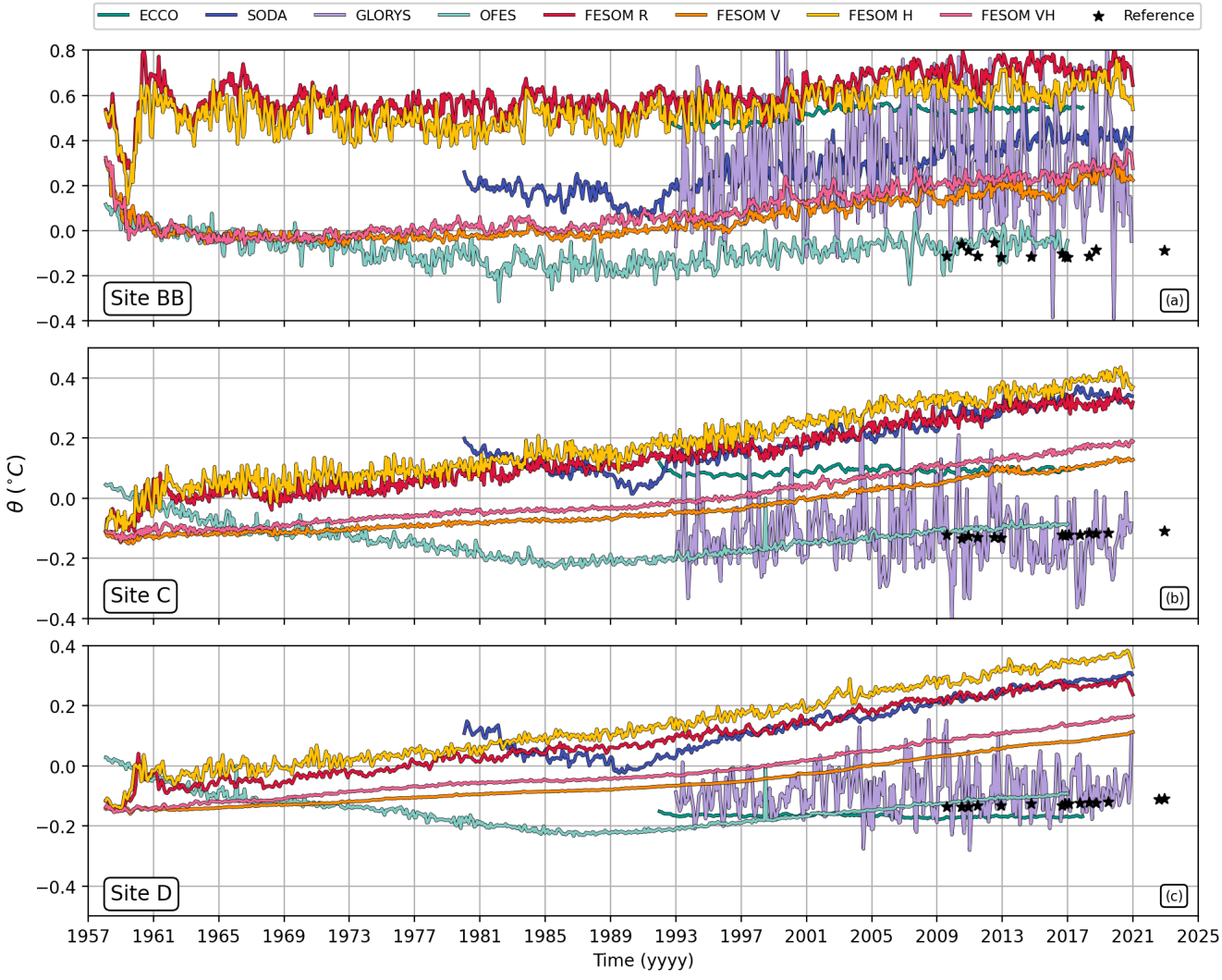

Figure 6. Time series of potential temperature (θ) at the grid point closest to Site BB (a), Site C (b), and Site D (c) for each simulation and for the reference (black stars), corresponding to the deepest CTD bin at each site. The color scheme follows Fig. 5.

of warmer waters across most of the basin. Waters entering the Brazil Basin are markedly warm, closely resembling the patterns obtained with ECCO (Fig. 2b) and SODA (Fig. 2c).

The bias field of FESOM R (Fig. 7f) shows widespread positive temperature biases, consistent with the warm anomalies in SODA (Fig. 2g). A key difference, however, lies in the spatial structure: whereas SODA shows a relatively uniform warm bias across the Argentine and Brazil Basins, FESOM R displays a pronounced discontinuity between them, with stronger positive anomalies in the Brazil Basin. Despite this overall positive anomaly, the inter-basin contrast in FESOM R resembles

https://doi.org/10.5194/egusphere-2026-2319
Preprint. Discussion started: 5 May 2026

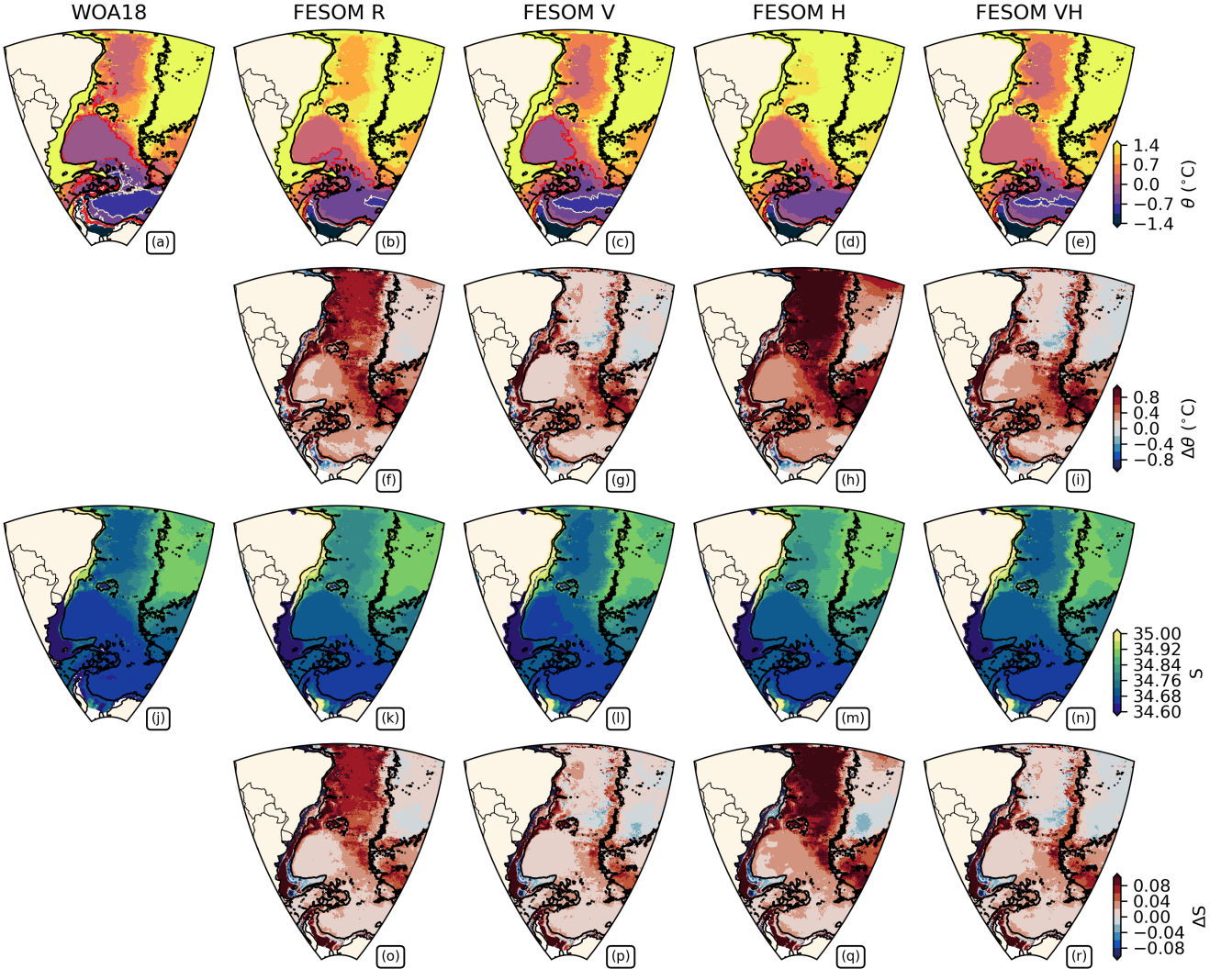

Figure 7. Total mean potential temperature (θ; panels a–e) and salinity (panels j–n) from 1994 to 2005 at the deepest valid level at each horizontal grid point, and the corresponding mean biases relative to WOA18 ($\Delta\theta$, panels f–i; ΔS, panels o–r). Columns correspond to WOA18 (reference), FESOM R, FESOM V, FESOM H, and FESOM VH, from left to right. The black contour indicates the 3000 m isobath, the red contour marks the $\theta = 0.0^{\circ}$C isotherm, and the white contour marks the $\theta = -0.7^{\circ}$C isotherm.

the patterns observed in ECCO (Fig. 2f) and OFES (Fig. 2i), but with an important distinction: in ECCO and OFES, the contrast results from a reversal in the sign of the bias between basins, whereas in FESOM R the discontinuity reflects only a change in magnitude, as the bias remains positive throughout. FESOM R also exhibits a negative temperature anomaly along the eastern side of the Antarctic Peninsula, consistent with the patterns found in all previous simulations except ECCO.

https://doi.org/10.5194/egusphere-2026-2319
Preprint. Discussion started: 5 May 2026

FESOM V (Fig. 7c) shows a substantial improvement relative to FESOM R. A broader area of the central Weddell Sea is occupied by cold waters with $\theta \leq -0.7°C$, though these waters still do not extend into the Scotia Sea. Waters with $\theta \leq 0.0°C$ now span the entire Argentine Basin, and a colder class of waters flows from this basin into the Brazil Basin, comparable to the pattern obtained with GLORYS (Fig. 2d). The bias map (Fig. 7g) reflects this improvement, displaying reduced magnitudes and a more spatially uniform warm bias across the study region, without the basin discontinuities present in FESOM R.

FESOM H (Fig. 7d) exhibits the weakest performance among the four experiments. No waters colder than $-0.7°C$ are present in the central Weddell Sea, and waters colder than $0.0°C$ are absent in the Argentine Basin. A warmer class of waters, relative to both FESOM R and FESOM V, is exported northward into the Brazil Basin, resembling the pattern observed in SODA (Fig. 2c) but with higher temperatures. The bias field (Fig. 7h) displays spatial patterns similar to those of FESOM R but with substantially larger magnitudes, resulting in a poorer representation of inter-basin connectivity.

FESOM VH (Fig. 7e) performs better than FESOM R in some aspects but worse in others. Waters colder than $-0.7°C$ occupy a broader area of the central Weddell Sea, and a colder class of waters flows from the Argentine Basin into the Brazil Basin, indicating an improved representation in that region. However, the connection between the Weddell Sea and the Argentine Basin remains poorly represented, as waters colder than $0.0°C$ are not exported northward from the Scotia Sea, unlike in FESOM R and FESOM V. The bias field (Fig. 7i) shows spatial patterns similar to those of FESOM H, but with larger magnitudes.

Conceptually, the relationship between FESOM H and FESOM VH mirrors that between FESOM R and FESOM V: both pairs share the same horizontal resolution, with the latter in each pair incorporating enhanced vertical resolution. In both cases, increasing vertical resolution produces a more realistic representation of abyssal water masses and their northward spreading, whereas horizontal refinement alone appears to have the opposite effect. This degradation may be linked to the representation of subgrid-scale processes: while diffusivity for the GM parameterization scales linearly with horizontal resolution, this may not sufficiently suppress the eddy parameterization in regions where resolution is fine enough to partially resolve eddies.

The spatial patterns described for θ are largely mirrored in the salinity fields (Fig. 7j–r), and as a consequence, the σ_4 field (Fig. S4) displays predominantly negative biases across most of the analyzed regions, indicating that density variations are primarily controlled by temperature rather than salinity. Over the Antarctic continental shelf, density biases are positive, in contrast to the negative values observed elsewhere. Despite the presence of relatively dense waters on the shelf, these waters are not sufficiently transferred to the abyssal Weddell Sea through downslope cascading, limiting the ventilation of the deep basin and contributing to the negative density biases observed in this region.

The supplementary videos support this picture, as no clear indications of dense shelf waters reaching the abyssal Weddell Sea can be seen in any of the configurations. Unlike the previously analyzed products, the FESOM simulations do not exhibit inverse density trends between adjacent basins. Instead, all experiments display a general negative density trend across the Weddell Sea, Argentine, and Brazil Basins, though the rates of change differ among configurations. In the Weddell Sea, FESOM R and FESOM H lose all waters within the density range $46.16 < \sigma_4 < 46.20$ kg m^{-3} by 2019, whereas FESOM V and FESOM VH do not completely lose this density class, though its volume decreases over time. In the Argentine Basin, FESOM R loses all waters within $46.08 < \sigma_4 < 46.12$ kg m^{-3} by 1993, FESOM V by 2002, FESOM H by 1988, and FESOM VH by 1995. In the Brazil Basin, FESOM R and FESOM H lose all waters within $46.04 < \sigma_4 < 46.08$ kg m^{-3} by 1968, while FESOM V

https://doi.org/10.5194/egusphere-2026-2319
Preprint. Discussion started: 5 May 2026

and FESOM VH retain this density class throughout the simulation. These results indicate that enhanced vertical resolution promotes a more coherent density evolution across connected basins.

Taken together, the FESOM experiments indicate that enhancing vertical resolution substantially improves the representation of abyssal water masses, producing colder and denser bottom waters and a more continuous connection between the Weddell Sea and the downstream basins. In contrast, increasing horizontal resolution alone does not improve the representation of abyssal properties and may even amplify existing biases. It should be noted that no adjustments were made to the mixing parameterizations in any of the experiments, and the degradation observed in the horizontally refined configurations may partly reflect this. Investigating the interaction between grid resolution and mixing parameterizations is beyond the scope of the present study, which focuses on the isolated and combined effects of grid resolution changes.

4.2 TS diagram analysis

In the Argentine Basin, FESOM R shows a clear absence of waters colder than 0.0°C, with maximum densities reaching only around 45.92 kg m^{-3} (Fig. 8c), and a saltier–warmer bias along these density levels relative to the reference (Fig. 8d). In the Brazil Basin, the absence of cold and dense water classes is even more pronounced, with minimum temperatures around 1.0°C and maximum densities near 45.84 kg m^{-3} (Fig. 8e and f), indicating a poor representation of the connection between the two basins.

FESOM V shows subtle but notable changes relative to FESOM R in the Argentine Basin: temperatures now reach 0.0°C and waters with densities exceeding 45.92 kg m^{-3} are present, unlike in FESOM R where densities remain at or just above this value, though the saltier–warmer bias along density levels persists (Fig. 8g and h). In the Brazil Basin, a colder and denser class of waters now occupies the deepest part of the water column, with properties similar to those found in the reference (Fig. 8i). This indicates an improved connection between the two basins, with the θ–S curves lying much closer to the reference and nearly overlapping (Fig. 8j).

FESOM H shows a θ–S distribution in the Argentine Basin very similar to that of FESOM R (Fig. 8k and l). In the Brazil Basin, however, the deviation from the reference is even larger than in FESOM R, with a greater loss of cold waters, a shift of the distribution toward lighter densities, and a higher concentration of warm points (Fig. 8m and n). This indicates that increasing horizontal resolution without modifying vertical resolution does not improve the representation of abyssal waters and can even degrade it.

FESOM VH closely resembles FESOM V in both the Argentine and Brazil Basins (Fig. 8o–r), with only minor differences in the θ–S distribution. Compared to FESOM H, FESOM VH recovers most of the improvement associated with enhanced vertical resolution, but the additional horizontal refinement does not substantially alter the θ–S relationship relative to FESOM V. These results confirm that vertical refinement provides consistent improvements in the representation of abyssal waters, whereas horizontal refinement alone has mixed or detrimental effects.

Overall, the θ–S analysis confirms that vertical resolution is the dominant factor controlling the representation of abyssal water properties and inter-basin connectivity. Refining the vertical grid consistently improves the density structure and the

https://doi.org/10.5194/egusphere-2026-2319
Preprint. Discussion started: 5 May 2026

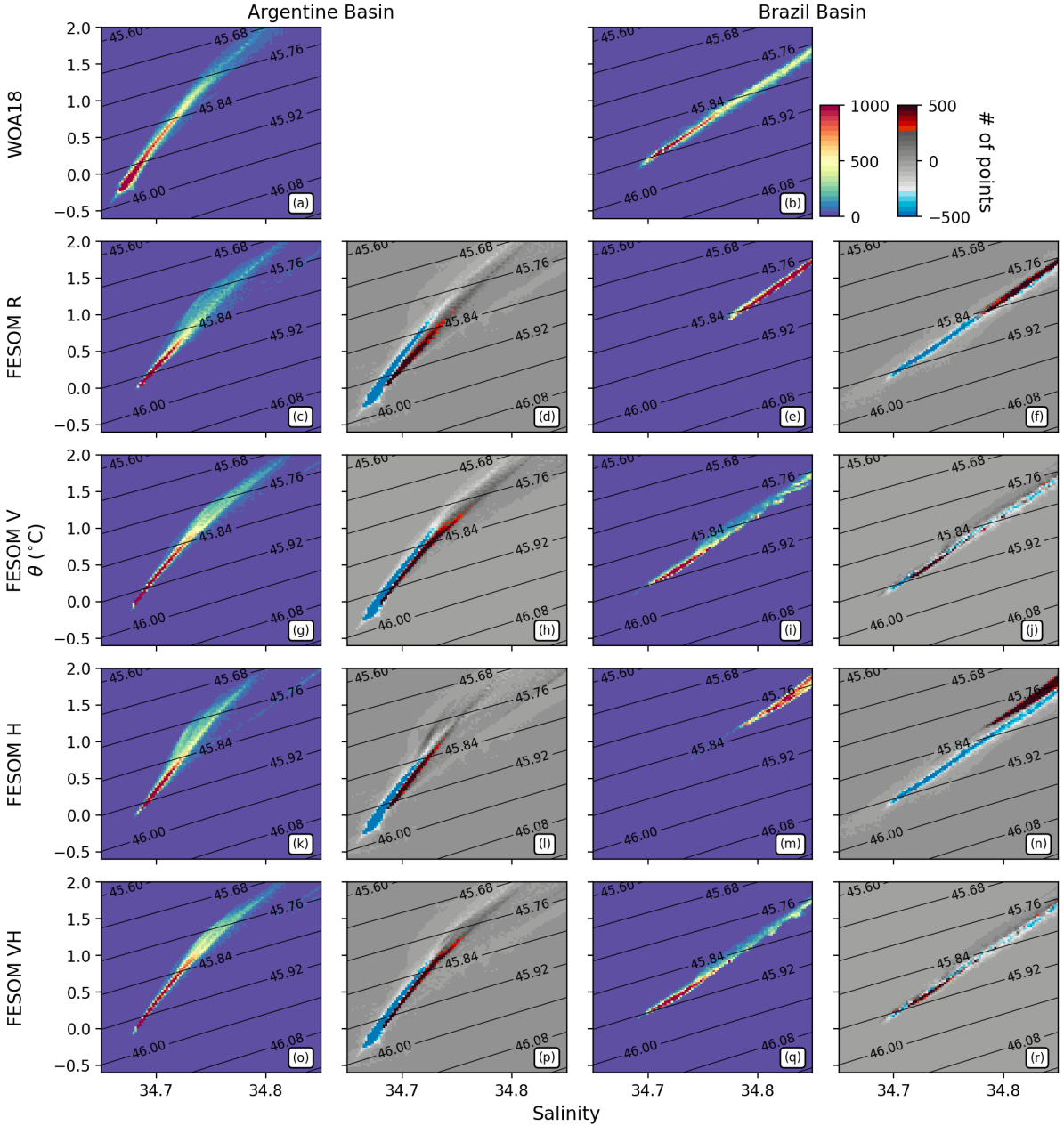

Figure 8. Time averaged θ–S distribution of the Argentine Basin (first column) and of the Brazil Basin (third column). Averaged θ–S distribution of the difference between WOA and each simulation at the Argentine Basin (second column) and at the Brazil Basin (fourth column). The rows from top to bottom represent WOA18 (first row), FESOM R (second row), FESOM V (third row), FESOM H (fourth row), and FESOM VH (fifth row). Contour lines are σ_4. The diagrams are zoomed to the abyssal layer ($-0.6^\circ\mathrm{C} < \theta < 2.0^\circ\mathrm{C}$; $34.65 < S < 34.85$).

https://doi.org/10.5194/egusphere-2026-2319
Preprint. Discussion started: 5 May 2026

connection between the Argentine and Brazil Basins, whereas horizontal refinement alone does not yield comparable benefits and can even degrade the results.

4.3 Temperature distribution across Vema Channel

In FESOM R (Fig. 4f), the Vema Channel is represented but remains poorly resolved, consistent with the goal of replicating the configurations of the previously assessed products. Only a few grid points fall inside the channel, and the deepest ones do not reach its full depth, with minimum temperatures staying above 0.0°C. In FESOM V (Fig. 4g), the channel structure becomes more clearly defined and the deepest parts contain colder water than in FESOM R, including temperatures below 0.0°C, though the amount of very cold water remains limited. FESOM H (Fig. 4h), in contrast, although offering a more detailed geometric description of the channel than the reference, does not improve the abyssal thermal structure: bottom waters remain warmer than in both FESOM R and FESOM V, and the coldest isotherms bend upward toward the western side of the channel, inconsistent with the expected structure.

FESOM VH (Fig. 4i), which combines the enhanced vertical resolution from FESOM V and the finer horizontal grid of FESOM H, restores and extends the improvements obtained with higher vertical resolution. The coldest isotherms are again present within the channel, and the bottom water layer bends toward the eastern wall. This eastward displacement of the cold core is consistent with *in situ* observations of the AABW flow through the Vema Channel (Morozov et al., 2018), which describe a bottom-intensified current steered along the eastern flank. The mechanism behind this deflection has been attributed to the Ekman flux induced by bottom friction, which drives a lateral shift of the densest water mass toward the eastern boundary. This feature is also reproduced in regional numerical simulations of AABW flow (Frey et al., 2019), where the cold core similarly adheres to the eastern wall while maintaining a narrow bottom-intensified jet. The presence of this structure in FESOM VH therefore indicates that the combined refinements enable the model to reproduce both the cold core and its realistic eastward deflection, though waters colder than 0.0°C remain absent.

These results show that vertical resolution is the key factor enabling the representation of cold abyssal waters within the Vema Channel, whereas horizontal refinement alone distorts the thermal structure without recovering the coldest water masses. The combined refinement of both grids, however, goes beyond simply improving the temperature field: it also allows the model to reproduce the eastward deflection of the AABW core, a dynamical feature that cannot be captured without sufficient resolution in both dimensions. As in the previous subsections, no adjustments were made to the mixing parameterizations, and the degradation observed in FESOM H may partly reflect this limitation.

4.4 Comparison with *in situ* data

During the CLIVAR period (Fig. 5a and d), FESOM R shows the highest correlation among the four experiments, but its mean temperature substantially overestimates the reference. FESOM V, despite a near-zero correlation, reproduces the observed variability more faithfully and exhibits a smaller warm bias, with a mean temperature close to the reference. FESOM H displays weak correlation and the largest warm bias among the four configurations. FESOM VH improves upon FESOM H

https://doi.org/10.5194/egusphere-2026-2319
Preprint. Discussion started: 5 May 2026

in both correlation and mean temperature, performing similarly to FESOM V. Overall, the vertically refined configurations (FESOM V and VH) better capture the temperature structure in the channel than those with horizontal refinement alone.

During the E2 period (Fig. 5b and e), FESOM V achieves the highest correlation among the four experiments, with small variability, a near-zero RMSE, and the smallest warm bias, making it the configuration most similar to the reference. FESOM VH also shows small variability and RMSE, but with a worse correlation than FESOM V. FESOM R shows a lower correlation and larger variability, while FESOM H remains the warmest and most variable configuration. As in the CLIVAR period, the vertically refined configurations outperform those with horizontal refinement alone.

During the SAMBA period (Fig. 5c and f), FESOM V and VH remain consistently closer to the reference than FESOM R and H, both in mean temperature and variability. FESOM H shows the largest warm bias and variability, while FESOM V and VH exhibit smaller biases and RMSE values. Regarding correlation, FESOM R achieves the highest value among the four configurations, while FESOM H shows a slightly negative value.

Across all three mooring periods, vertical resolution consistently emerges as the key factor controlling model performance. FESOM V and VH systematically reduce warm biases and better reproduce the observed variability, while FESOM H introduces larger deviations relative to FESOM R. Although model skill varies across periods, the contrast between vertically and horizontally refined configurations remains robust throughout.

The simulations were also compared with CTD data from the SAMBA-West array at Sites BB, C, and D (Table 3, Fig. 6). At Site BB, all FESOM configurations produce temperatures warmer than the reference, with FESOM V providing the closest match and FESOM R the largest deviation. The observed CTD trend at this site is not statistically significant, which excludes a meaningful comparison of warming trends with the simulations.

At Sites C and D, FESOM V again provides the closest representation of the reference mean temperature, while FESOM H shows the largest deviations. FESOM VH performs comparably to FESOM V in terms of mean temperature, while FESOM R shows intermediate values. Regarding trends, all configurations overestimate the observed warming, with FESOM H showing the largest overestimation and FESOM R the smallest. These results confirm that enhanced vertical resolution is the primary factor driving improvement in the representation of abyssal temperatures along the SAMBA-West line, while horizontal refinement alone has little systematic benefit.

Taken together, the comparison with *in situ* data reinforces the conclusions drawn from the previous subsections: vertical resolution is the dominant factor controlling the representation of abyssal water properties in the Vema Channel and along the SAMBA-West array, while horizontal refinement alone does not yield systematic improvements and can even degrade model performance.

5 Conclusions

This study evaluates three ocean reanalyses and one forward ocean model to identify shared and model-specific biases in the representation of the abyssal ocean, and uses these results to motivate four targeted experiments with FESOM 2, in which horizontal and vertical grid resolution are modified independently and in combination. The analysis focuses on the connec-

https://doi.org/10.5194/egusphere-2026-2319
Preprint. Discussion started: 5 May 2026

tivity between the Argentine and Brazil Basins through the Vema Channel, while also considering the upstream link with the Antarctic continental slope and the abyssal Weddell Sea.

ECCO, SODA, GLORYS, and OFES broadly reproduce the large-scale thermohaline structure of the abyssal South Atlantic but exhibit both recurring and model-specific inconsistencies. ECCO and OFES show alternating bias signs between the Weddell Sea and the Argentine and Brazil Basins, suggesting difficulties in maintaining inter-basin continuity, whereas GLORYS and SODA display a persistent warm and saline bias throughout the system. Across all simulations, temperature errors dominate the density discrepancies, indicating that inaccuracies in the thermal field are the primary driver of the simulated biases. None of the evaluated simulations clearly captures the downslope cascading of dense shelf waters from the Antarctic continental shelf, and the temporal evolution of abyssal density reveals inconsistencies between basins, with some simulations showing a progressive increase in density within the Weddell Sea while the downstream basins exhibit opposite or disconnected trends. These results point to limitations in the representation of deep-basin connectivity and the propagation of abyssal water mass signals across the system.

The FESOM experiments indicate that enhancing vertical resolution is the most effective modification to improve the representation of abyssal waters. Finer vertical resolution reduces temperature biases, improves the continuity of water-mass properties across the Weddell Sea, Argentine, and Brazil Basins, and slows the loss of the densest abyssal water classes over time, resulting in a more stable and coherent representation of abyssal water masses and their inter-basin propagation.

In contrast, increasing horizontal resolution alone does not lead to systematic improvements, which is consistent with previous multi-model assessments (Chassignet et al., 2020). In several cases, horizontal refinement results in warmer abyssal layers. One possible explanation is that changes in horizontal resolution alter the balance between resolved and parameterized mesoscale eddy activity, as scaling diffusivity linearly with horizontal resolution may not sufficiently suppress the eddy parameterization in regions where the grid is fine enough to partially resolve eddies. These results suggest that recalibrating mixing parameterizations when modifying horizontal resolution may be necessary, particularly in eddy-permitting regimes, though investigating this interaction is beyond the scope of the present study.

When both vertical and horizontal refinements are applied together, the model reproduces certain local features more realistically, including the cold core of the AABW and its eastward displacement within the Vema Channel. However, the overall temperature field remains warmer than in the vertically refined case alone, and the large-scale abyssal properties become slightly less consistent with the observational reference. The combined refinement therefore improves specific local dynamical features but does not translate into a basin-scale thermohaline improvement.

Overall, these results highlight the dominant role of vertical resolution in controlling the large-scale representation of abyssal water properties and inter-basin connectivity. Horizontal refinement, whether applied alone or in combination with vertical refinement, does not systematically improve the large-scale thermohaline structure and may even degrade it. Further improvements will likely require a careful treatment of the interaction between grid resolution and mixing parameterizations, particularly as models transition into eddy-permitting regimes.

https://doi.org/10.5194/egusphere-2026-2319
Preprint. Discussion started: 5 May 2026

Appendix A

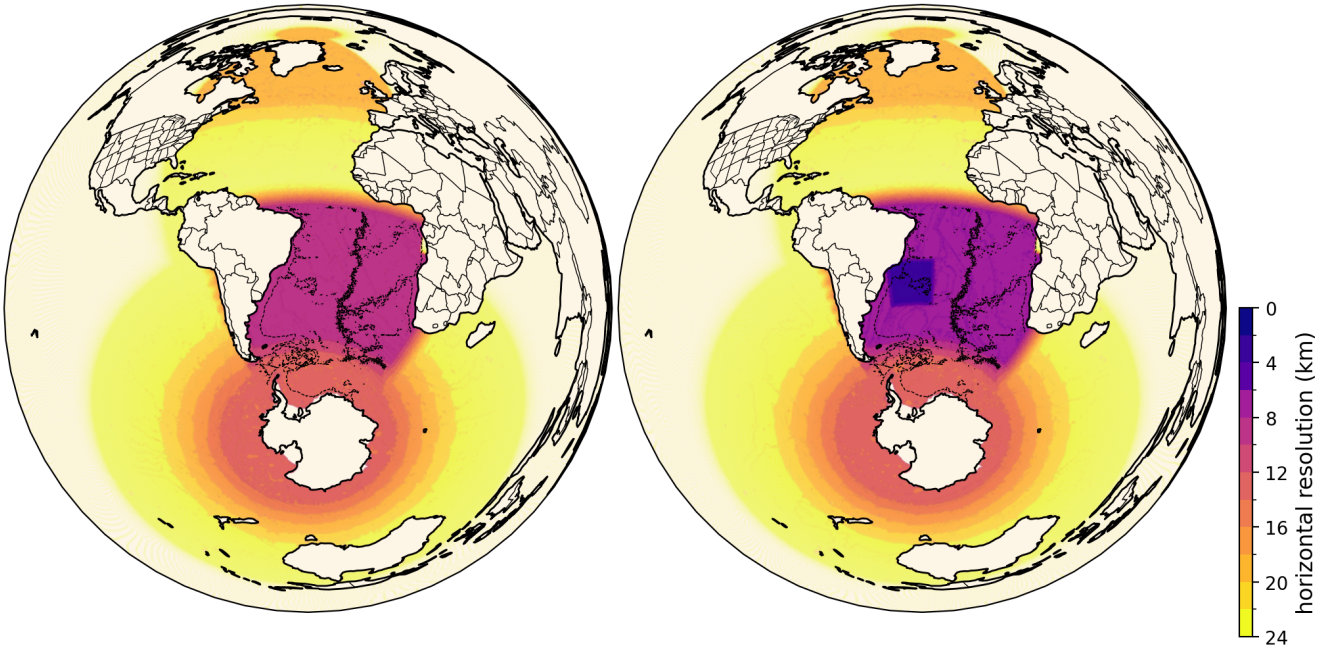

Figure A1. Panel a) Square root of grid-cell area (FESOM R and FESOM V) of the entire globe. Panel b) Same as panel a, but of FESOM H and FESOM VH. Dashed black contour marks the isobath of 3000 m and solid black contour the continents.

https://doi.org/10.5194/egusphere-2026-2319
Preprint. Discussion started: 5 May 2026

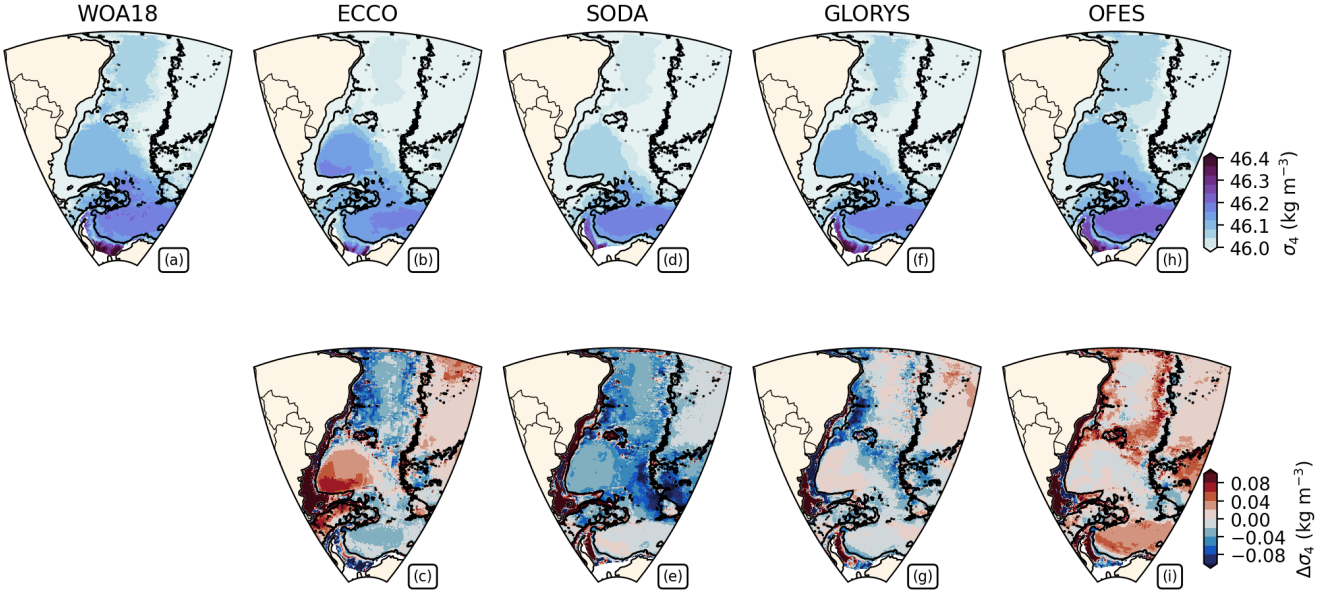

Figure B1. Total mean potential density referenced to 4000 m (σ_4) from 1994 to 2005 at the deepest valid level at each horizontal grid point (upper panels) and the corresponding mean bias relative to the reference (simulation minus WOA18). The black contour indicates the 3000 m isobath.

https://doi.org/10.5194/egusphere-2026-2319
Preprint. Discussion started: 5 May 2026

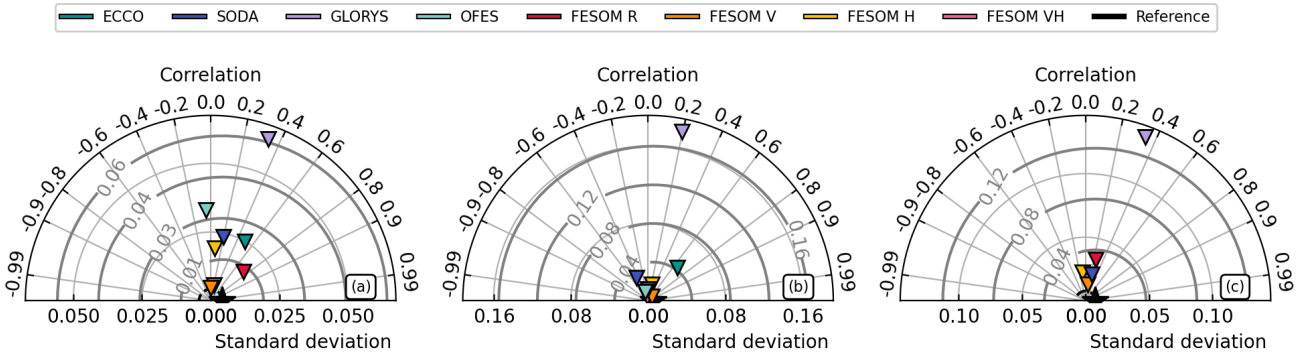

Figure C1. Taylor diagrams comparing temperature records from the CLIVAR (a), E2 (b), and SAMBA (c) moorings with model simulations within the Vema Channel. The simulations are ECCO (teal), SODA (indigo), GLORYS (lavender purple), OFES (light teal), FESOM R (crimson), FESOM V (orange), FESOM H (amber), and FESOM VH (coral pink).

https://doi.org/10.5194/egusphere-2026-2319
Preprint. Discussion started: 5 May 2026

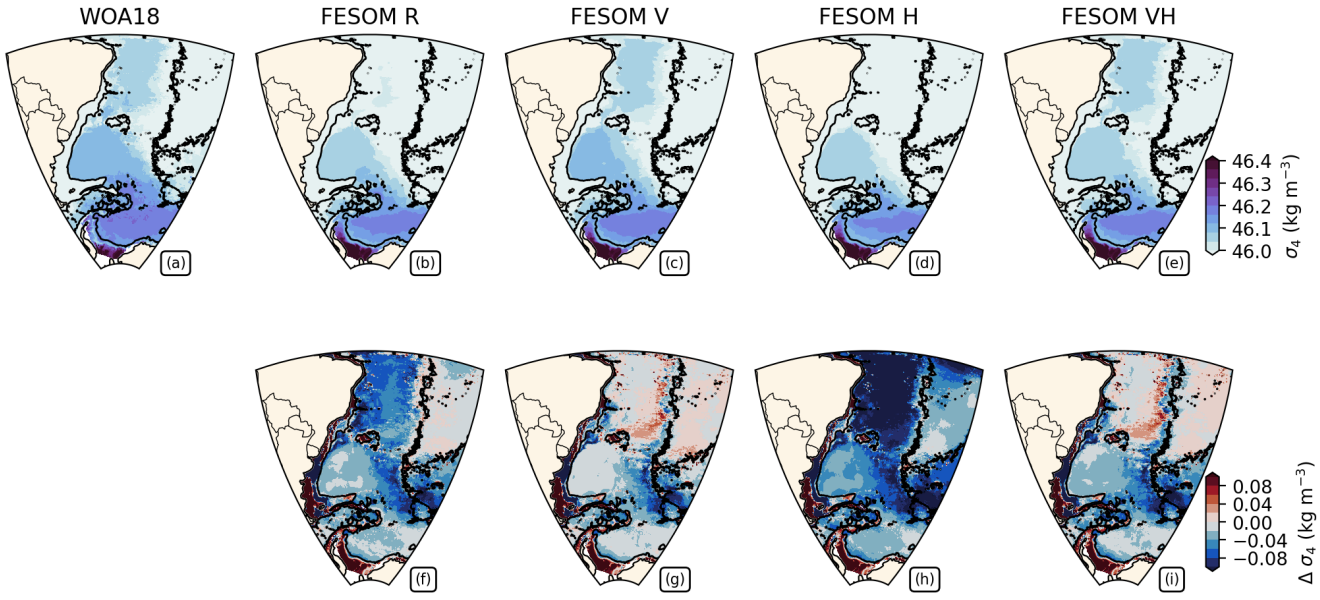

Figure D1. Total mean potential density referenced to 4000 m (σ_4) from 1994 to 2005 at the deepest valid level at each horizontal grid point (upper panels) and the corresponding mean bias relative to the reference (simulation minus WOA18). The black contour indicates the 3000 m isobath.

Data availability. The WOA18 climatology is freely available at https://www.ncei.noaa.gov/access/world-ocean-atlas-2018/. ECCO Version 4 Release 4 outputs are available at https://podaac.jpl.nasa.gov/dataset/ECCO_L4_TEMP_SALINITY_LLC0090GRID_MONTHLY_V4R4. SODA version 3.4.2m outputs were downloaded from https://dsrs.atmos.umd.edu/DATA/soda3.4.2/REGRIDED/ocean/. GLORYS reanalysis outputs are available through the Copernicus Marine Service at https://data.marine.copernicus.eu/product/GLOBAL_MULTIYEAR_PHY_001_030/services. OFES2 outputs are distributed through the GrADS Data Server and are available at https://www.jamstec.go.jp/ofes/ofes2.html. The hydrographic data from the SAMBA-West array and from the MSM60 cruise are described in Santos et al. (2025). The mooring data are described in Zenk (2008), Zenk and Visbeck (2013), and Campos et al. (2021). The FESOM2 simulation outputs are archived in Zenodo and organized into thematic datasets. Outputs associated with the Vema section (DOI: 10.5281/zenodo.19595306), TS diagrams (DOI: 10.5281/zenodo.19597204), PIES (DOI: 10.5281/zenodo.19597367), and mooring analyses (DOI: 10.5281/zenodo.19597574) are each provided under dedicated DOIs. Abyssal property fields are further subdivided by experiment: FESOM R (DOI: 10.5281/zenodo.19598232), FESOM V (DOI: 10.5281/zenodo.19597878), FESOM H (DOI: 10.5281/zenodo.19597860), and FESOM VH (DOI: 10.5281/zenodo.19597737), with each experiment archived under its own DOI.

https://doi.org/10.5194/egusphere-2026-2319
Preprint. Discussion started: 5 May 2026

Video supplement. Video supplements showing the temporal evolution of potential density referenced to 4000 m depth (σ_4) at the deepest valid level for each simulation are archived in Zenodo under the DOI: 10.5281/zenodo.19699061.

Author contributions. **Daniel M. C. Santos**: Conceptualization (lead); Data Curation (lead); Formal Analysis (lead); Investigation (lead); Software (equal); Validation (lead); Visualization (lead); Writing – Original Draft Preparation (lead). **Mathias Van Caspel**: Conceptualization (supporting); Software (equal); Validation (supporting); Supervision (supporting); Writing - Review & Editing (supporting). **Ralph Timmermann**: Resources (lead); Supervision (supporting); Writing - Review & Editing (lead). **Olga T. Sato**: Conceptualization (supporting); Funding Acquisition (lead); Project Administration (lead); Supervision (lead); Writing - Review & Editing (supporting).

Competing interests. The authors declare that they have no conflict of interest.

Acknowledgements. This research was supported by FAPESP [2017/09659-6, 2021/09317-3, and 2023/11774-9], as well as by the project Ocean Cryosphere Exchanges in ANtarctica: Impacts on Climate and the Earth System (OCEAN ICE), funded by the European Union's Horizon Europe Research and Innovation Programme under grant agreement No. 101060452 (https://doi.org/10.3030/101060452). OCEAN ICE contribution number 52. During the preparation of this work, the authors used ChatGPT and Claude to improve the readability and language of the manuscript. After using this tool, the authors reviewed and edited the content as needed and assume full responsibility for the content of the published article.

https://doi.org/10.5194/egusphere-2026-2319
Preprint. Discussion started: 5 May 2026

References

Abrahamsen, E. P., Meijers, A. J., Polzin, K. L., Naveira Garabato, A. C., King, B. A., Firing, Y. L., Sallée, J.-B., Sheen, K. L., Gordon, A. L., Huber, B. A., et al.: Stabilization of dense Antarctic water supply to the Atlantic Ocean overturning circulation, Nature Climate Change, 9, 742–746, 2019.

Arhan, M., Heywood, K. J., and King, B. A.: The deep waters from the Southern Ocean at the entry to the Argentine Basin, Deep Sea Research Part II: Topical Studies in Oceanography, 46, 475–499, 1999.

Bailey, S. T., Jones, C. S., Abernathey, R. P., Gordon, A. L., and Yuan, X.: Water mass transformation variability in the Weddell Sea in ocean reanalyses, Ocean Science, 19, 381–402, 2023.

Boyer, T. P., Antonov, J. I., Baranova, O. K., Garcia, H. E., Johnson, D. R., Mishonov, A. V., O'Brien, T. D., Seidov, D., Smolyar, I., Zweng, M. M., et al.: World Ocean Database 2013, NOAA Atlas NESDIS 72, Silver Spring, MD, 209 pp., http://doi.org/10.7289/V5NZ85MT, 2013.

Campos, E. J., Van Caspel, M. C., Zenk, W., Morozov, E. G., Frey, D. I., Piola, A. R., Meinen, C. S., Sato, O. T., Perez, R. C., and Dong, S.: Warming trend in Antarctic Bottom Water in the Vema Channel in the South Atlantic, Geophysical Research Letters, 48, e2021GL094 709, 2021.

Carmack, E. C.: Water characteristics of the Southern Ocean south of the Polar Front., A Vouage of Discovery, pp. 15–41, 1977.

Carton, J. A., Chepurin, G. A., and Chen, L.: SODA3: A new ocean climate reanalysis, Journal of Climate, 31, 6967–6983, 2018.

Chassignet, E. P., Yeager, S. G., Fox-Kemper, B., Bozec, A., Castruccio, F., Danabasoglu, G., Ferrari, R., Forget, G., Hecht, M. W., Holland, M. M., Kim, W., Koldunov, N. V., Li, Y., Lin, P., Liu, H., Nurser, A. J. G., Small, J., Tsujino, H., and Yeager, D.: Impact of horizontal resolution on global ocean–sea ice model simulations based on the experimental protocols of the Ocean Model Intercomparison Project phase 2 (OMIP-2), Geoscientific Model Development, 13, 4595–4637, https://doi.org/10.5194/gmd-13-4595-2020, 2020.

Chidichimo, M. P., Piola, A. R., Meinen, C. S., Perez, R., Campos, E. J. D., Dong, S., Lumpkin, R., and Garzoli, S.: Brazil Current Volume Transport Variability during 2009–2015 from a long-term moored array at 34.5 S, Journal of Geophysical Research: Oceans, 126, e2020JC017 146, 2021.

Chidichimo, M. P., Perez, R. C., Speich, S., Kersalé, M., Sprintall, J., Dong, S., Lamont, T., Sato, O. T., Chereskin, T. K., Hummels, R., et al.: Energetic overturning flows, dynamic interocean exchanges, and ocean warming observed in the South Atlantic, Communications Earth & Environment, 4, 10, 2023.

Cunningham, S. A., Kanzow, T., Rayner, D., Baringer, M. O., Johns, W. E., Marotzke, J., Longworth, H. R., Grant, E. M., Hirschi, J. J.-M., Beal, L. M., et al.: Temporal variability of the Atlantic meridional overturning circulation at 26.5 N, science, 317, 935–938, 2007.

Danilov, S., Wang, Q., Timmermann, R., Iakovlev, N., Sidorenko, D., Kimmritz, M., Jung, T., and Schröter, J.: Finite-element sea ice model (FESIM), version 2, Geoscientific Model Development, 8, 1747–1761, 2015.

Danilov, S., Sidorenko, D., Wang, Q., and Jung, T.: The finite-volume sea ice–ocean model (fesom2), Geoscientific Model Development, 10, 765–789, 2017.

Dee, D. P., Uppala, S. M., Simmons, A. J., Berrisford, P., Poli, P., Kobayashi, S., Andrae, U., Balmaseda, M., Balsamo, G., Bauer, d. P., et al.: The ERA-Interim reanalysis: Configuration and performance of the data assimilation system, Quarterly Journal of the royal meteorological society, 137, 553–597, 2011.

https://doi.org/10.5194/egusphere-2026-2319
Preprint. Discussion started: 5 May 2026

Delworth, T. L., Rosati, A., Anderson, W., Adcroft, A. J., Balaji, V., Benson, R., Dixon, K., Griffies, S. M., Lee, H.-C., Pacanowski, R. C., et al.: Simulated climate and climate change in the GFDL CM2. 5 high-resolution coupled climate model, Journal of Climate, 25, 2755–2781, 2012.

Donea, J. and Huerta, A.: Finite element methods for flow problems, John Wiley & Sons, 2003.

ECCO Consortium, Fukumori, I., Wang, O., Fenty, I., Forget, G., Heimbach, P., and Ponte, R. M.: ECCO Central Estimate (Version 4 Release 4), https://podaac.jpl.nasa.gov/dataset/ECCO_L4_TEMP_SALINITY_LLC0090GRID_MONTHLY_V4R4 (last access: 17 July 2025), 2025.

Fahrbach, E., Rohardt, G., Scheele, N., Schröder, M., Strass, V., and Wisotzki, A.: Formation and discharge of deep and bottom water in the northwestern Weddell Sea, journal = Journal of Marine Research, 1995.

Forget, G., Campin, J.-M., Heimbach, P., Hill, C. N., Ponte, R. M., and Wunsch, C.: ECCO version 4: An integrated framework for non-linear inverse modeling and global ocean state estimation, Geoscientific Model Development, 8, 3071–3104, 2015.

Frey, D., Morozov, E., Fomin, V., Diansky, N., and Tarakanov, R.: Regional modeling of Antarctic Bottom Water flows in the key passages of the Atlantic, Journal of Geophysical Research: Oceans, 124, 8414–8428, 2019.

Fukumori, I., Wang, O., Fenty, I., Forget, G., Heimbach, P., and Ponte, R. M.: ECCO version 4 release 3, Tech. rep., Jet Propulsion Laboratory (JPL/NASA), 2017.

Gent, P. R. and Mcwilliams, J. C.: Isopycnal mixing in ocean circulation models, Journal of Physical Oceanography, 20, 150–155, 1990.

Heuzé, C.: Antarctic bottom water and North Atlantic deep water in CMIP6 models, Ocean Science Discussions, 2020, 1–38, 2020.

Hogg, N., Biscaye, P., Gardner, W., and Schmitz Jr, W. J.: On the transport and modification of Antarctic Bottom Water in the Vema Channel, Journal of Marine Research, 1982.

IOC, SCOR, and IAPSO: The International Thermodynamic Equation of Seawater – 2010: Calculation and Use of Thermodynamic Properties, no. 56 in Manuals and Guides, Intergovernmental Oceanographic Commission, 2010.

Jean-Michel, L., Eric, G., Romain, B.-B., Gilles, G., Angélique, M., Marie, D., Clément, B., Mathieu, H., Olivier, L. G., Charly, R., et al.: The Copernicus global 1/12 oceanic and sea ice GLORYS12 reanalysis, Frontiers in Earth Science, 9, 698 876, 2021.

Johnson, G. C.: Antarctic Bottom Water Warming and Circulation Slowdown in the Argentine Basin From Analyses of Deep Argo and Historical Shipboard Temperature Data, Geophysical Research Letters, 49, e2022GL100 526, 2022.

Karstensen, J., Speich, S., Asdar, S., Berbel, G. B. B., Branlard, L., Carvalho, A., Chidichimo, M. P., Cotrim da Cunha, L., da Silva Calixto, A., Edsgren, C., Guerrero, R., Hummels, R., Jones, S., Kersale, M., Lebehot, A., Marshall, T., Mohale, N., Rogge, A., Sato, O. T., Schrandt, J., Stöven, T., and Sutti Otera, B.: Seamount Observatory and SAMOC Overturning, Cruise No. MSM60, January 04 - February 01, 2017, Cape Town $SouthAfrica$ - Montevideo $Uruguay$, https://doi.org/10.2312/cr_msm60, 2019.

Kobayashi, S., Ota, Y., Harada, Y., Ebita, A., Moriya, M., Onoda, H., Onogi, K., Kamahori, H., Kobayashi, C., Endo, H., et al.: The JRA-55 reanalysis: General specifications and basic characteristics, Journal of the Meteorological Society of Japan. Ser. II, 93, 5–48, 2015.

Komori, N., Takahashi, K., Komine, K., Motoi, T., Zhang, X., and Sagawa, G.: Description of sea-ice component of coupled ocean–sea-ice model for the Earth Simulator (OIFES), J. Earth Simulator, 4, 31–45, 2005.

Large, W. G., McWilliams, J. C., and Doney, S. C.: Oceanic vertical mixing: A review and a model with a nonlocal boundary layer parameterization, Reviews of geophysics, 32, 363–403, 1994.

Locarnini, M., Mishonov, A., Baranova, O., Boyer, T., Zweng, M., Garcia, H., Seidov, D., Weathers, K., Paver, C., Smolyar, I., et al.: World ocean atlas 2018, volume 1: Temperature, 2018.

Madec, G. et al.: NEMO ocean engine. Note du Pôle de modélisation, Institut Pierre-Simon Laplace (IPSL), France, 27, 1288–1619, 2008.

https://doi.org/10.5194/egusphere-2026-2319
Preprint. Discussion started: 5 May 2026

Marshall, J., Hill, C., Perelman, L., and Adcroft, A.: Hydrostatic, quasi-hydrostatic, and nonhydrostatic ocean modeling, Journal of Geophysical Research: Oceans, 102, 5733–5752, 1997.

Meinen, C. S., Piola, A. R., Perez, R., and Garzoli, S.: Deep Western Boundary Current transport variability in the South Atlantic: Preliminary results from a pilot array at 34.5 S, Ocean Science, 8, 1041–1054, 2012.

Morozov, E., Frey, D., and Campos, E.: Flow of Antarctic bottom water in the Vema Channel. A review, Fundamentalnaya i Prikladnaya Gidrofizika, 11, 94–102, 2018.

Orsi, A. H., Johnson, G. C., and Bullister, J. L.: Circulation, mixing, and production of Antarctic Bottom Water, Progress in Oceanography, 43, 55–109, 1999.

Pacanowski, R. and Griffies, S.: The MOM3 manual. GFDL Ocean Group Tech. Rep. 4, NOAA, Geophysical Fluid Dynamics Laboratory, Princeton, NJ, 680, 1999.

Redi, M. H.: Oceanic isopycnal mixing by coordinate rotation, Journal of Physical Oceanography, 12, 1154–1158, 1982.

Santos, D. M., Biló, T. C., Napolitano, D. C., Perez, R. C., Polito, P. S., Gula, J., Dong, S., Campos, E. J., and Sato, O. T.: Antarctic bottom water contraction drives abyssal ocean warming along SAMBA-West line (34.5° S) in the Argentine basin, Deep Sea Research Part I: Oceanographic Research Papers, p. 104627, 2025.

Sasaki, H., Kida, S., Furue, R., Aiki, H., Komori, N., Masumoto, Y., Miyama, T., Nonaka, M., Sasai, Y., and Taguchi, B.: A global eddying hindcast ocean simulation with OFES2, Geoscientific Model Development, 13, 3319–3336, 2020.

Schott, F. A., Dengler, M., Zantopp, R., Stramma, L., Fischer, J., and Brandt, P.: The shallow and deep western boundary circulation of the South Atlantic at 5–11 S, Journal of Physical Oceanography, 35, 2031–2053, 2005.

Solodoch, A., Stewart, A., Hogg, A. M., Morrison, A., Kiss, A., Thompson, A., Purkey, S., and Cimoli, L.: How does antarctic bottom water cross the southern ocean?, Geophysical Research Letters, 49, e2021GL097 211, 2022.

Steele, M., Morley, R., and Ermold, W.: PHC: A global ocean hydrography with a high-quality Arctic Ocean, Journal of Climate, 14, 2079–2087, 2001.

Thacker, W. C. and Long, R. B.: Fitting dynamics to data, Journal of Geophysical Research: Oceans, 93, 1227–1240, 1988.

Valla, D., Piola, A. R., Meinen, C. S., and Campos, E.: Strong mixing and recirculation in the northwestern Argentine Basin, Journal of Geophysical Research: Oceans, 123, 4624–4648, 2018.

Wang, Q., Danilov, S., Sidorenko, D., Timmermann, R., Wekerle, C., Wang, X., Jung, T., and Schröter, J.: The Finite Element Sea Ice-Ocean Model (FESOM) v. 1.4: formulation of an ocean general circulation model, Geoscientific Model Development, 7, 663–693, 2014.

Wunsch, C. and Heimbach, P.: Practical global oceanic state estimation, Physica D: Nonlinear Phenomena, 230, 197–208, 2007.

Wunsch, C. and Heimbach, P.: Dynamically and kinematically consistent global ocean circulation and ice state estimates, in: International Geophysics, vol. 103, pp. 553–579, Elsevier, 2013.

Zenk, W.: Temperature fluctuations and current shear in Antarctic Bottom Water at the Vema Sill, Progress in Oceanography, 77, 276–284, 2008.

Zenk, W. and Visbeck, M.: Structure and evolution of the abyssal jet in the Vema Channel of the South Atlantic, Deep Sea Research Part II: Topical Studies in Oceanography, 85, 244–260, 2013.

Zweng, M. M., Reagan, J. R., Seidov, D., Boyer, T. P., Locarnini, R. A., Garcia, H. E., Mishonov, A. V., Baranova, O. K., Weathers, K. W., Paver, C. R., et al.: World ocean atlas 2018, volume 2: Salinity, 2019.